



## MASTER THESIS 2010

<b>Title:</b> Stabilization of two-phase flow in risers from reservoirs (anti-slug control).	<b>Subject (3-4 words):</b> Anti-slug control, Experiments, Flow regime map, OLGA
<b>Author:</b> Elisabeth Lovise Ringereide Hyllestad	<b>Carried out through:</b> 18.01.2010 – 14.06.2010
<b>Advisor:</b> Prof. Sigurd Skogestad <b>Co-advisors:</b> Prof. Ole Jørgen Nydal, Postdoc Weiwei Qiu, PhD student Esmail Jahanshahi	<u><b>Number of pages</b></u>  Hovedrapport: 76 Bilag: 19
<b>External advisor:</b>	
<b>ABSTRACT</b>  <b>Goal of work (key words):</b> The goal of this thesis was to study the dynamics of severe slugging through an experimental approach with a small-scale two-phase riser loop. A flow regime map was produced for an open-loop and closed-loop experiment. The controlled variable was the inlet pressure and the manipulated variable the top side valve opening. The goal was to see how a dynamic feedback controller could increase the production rate and extend the life-time of a reservoir. The dynamic controller was compared to choking the valve manually in a bifurcation map. The open-loop results were compared to a model constructed in OLGA.	
<b>Conclusions and recommendations (key words):</b> Severe slugging type I, which is the most severe case of slugging, occurred at low liquid and gas flow rates. The characteristics of this flow regime were large pressure amplitudes and long slugging-cycle periods. This flow regime was controlled by the dynamic controller as long as the gas flow rate was not too low, which caused the choke valve to close almost completely. Severe slugging type II occurred at higher liquid flow rates. Gas bubbles were able to penetrate the liquid blockage, breaking up the large liquid slugs. The pressure amplitude and the period decreased. This flow regime proved to be hard to control due to the high slugging frequency. However, this slugging type is less severe. A receiving facility can in most cases handle this flow type. Stabilizing severe slugging by manually choking the valve increased the back pressure compared to the dynamic controller. Elimination of severe slugging was attained when manually closing the valve to 10 % opening, while the dynamic controller stabilized the flow at 30 % opening.	
The riser model in OLGA produced compatible outputs to the experimental results. The similarity was highest for the experimental severe slugging type I region.	
I declare that this is an independent work according to the exam regulations of the Norwegian University of Science and Technology	
Date and signature: .....	



# Acknowledgements

During the course of this work, various people have contributed to achieving results and making this final time as a student a good experience. First I would like to thank the supervisor for this project, Professor Sigurd Skogestad, for always having the door open for questions and the great guidance throughout the work. Also, a thanks goes out to co-supervisor, Professor Ole Jørgen Nydal for interesting topic proposals and for good advise.

The experimental and simulation work was executed in collaboration with co-supervisor and post-doc Weiwei Qiu. I would like to thank her for a great teamwork and interesting discussions, in addition to creating a light and effective atmosphere throughout the many hours of lab work. Co-supervisor and Ph.D student Esmail Jahanshahi helped modify the miniloop and was available during the modeling work in OLGA and helped me understand the structure of the program.

I would like to thank Claudia Martins da Silva for including me in the Multiphase Lab meetings and providing the lab meeting minutes every week and Tor Kjeldby, for providing Weiwei Qiu and I with the PVT-table for air and water to use in the OLGA model of the miniloop.

Last I would like to thank my colleagues Dag-Erik Helgestad, Martin Buus Jensen and Anders Haukvik Røed for creating a healthy working environment at the office and for the company during coffee-brakes, and my parents for love and support during my time as a student.



# Contents

<b>Acknowledgements</b>	<b>iii</b>
<b>List of Figures</b>	<b>viii</b>
<b>List of Tables</b>	<b>ix</b>
<b>1 Introduction</b>	<b>1</b>
1.1 History and previous work . . . . .	1
1.2 Scope of work . . . . .	2
<b>2 Theory</b>	<b>5</b>
2.1 Flow regimes in two-phase pipelines . . . . .	5
2.1.1 Severe slugging definitions . . . . .	6
2.2 Control . . . . .	7
2.3 Anti-slug control . . . . .	10
<b>3 Experimental setup</b>	<b>11</b>
3.1 Comparison of results before and after modifications . . . . .	13
3.2 Equipment . . . . .	15
3.3 Calibration of equipment . . . . .	19
3.4 LabVIEW . . . . .	21
<b>4 Open-loop experiment</b>	<b>23</b>
4.1 Experimental . . . . .	23
4.2 Results and discussion . . . . .	24
4.2.1 Different flow regimes . . . . .	24
4.2.2 The severe slugging type I cycle . . . . .	31
4.2.3 Flow regime map . . . . .	34
4.2.4 Analysis of experimental data . . . . .	36
4.3 Sources of error . . . . .	39
<b>5 Closed-loop experiment</b>	<b>41</b>
5.1 Experimental . . . . .	41
5.1.1 Closed-loop flow regime map . . . . .	41
5.1.2 Bifurcation map . . . . .	41
5.2 Results and discussion . . . . .	42
5.2.1 Set point adjustment with P-control . . . . .	42
5.2.2 Filtering P1 measurements . . . . .	43
5.2.3 PD-control versus P-control . . . . .	43
5.2.4 Flow regime map with controller . . . . .	45

5.2.5	The gain of the controller . . . . .	48
5.2.6	Bifurcation map . . . . .	49
5.3	Sources of error . . . . .	51
<b>6</b>	<b>Comparison of experimental data with OLGA-model</b>	<b>53</b>
6.1	The model . . . . .	53
6.2	Results . . . . .	54
<b>7</b>	<b>Further work</b>	<b>61</b>
<b>8</b>	<b>Conclusion</b>	<b>63</b>
	<b>References</b>	<b>64</b>
<b>A</b>	<b>Raw data and calculations</b>	<b>67</b>
<b>B</b>	<b>Calibration Results and Calculations</b>	<b>69</b>
B.1	Real liquid flow velocity . . . . .	69
B.2	Calibration of liquid flow meter . . . . .	69
B.3	Pressure calibration . . . . .	70
<b>C</b>	<b>Calculation of frictional pressure drop in pipe between buffer tank and mixing point</b>	<b>73</b>
<b>D</b>	<b>Results and Calculation of the Flow Map</b>	<b>75</b>
D.1	Conversion to standard conditions . . . . .	75
<b>E</b>	<b>Deviation errors in the liquid flow velocities</b>	<b>77</b>
E.1	Deviation errors during liquid flow calibration . . . . .	77
E.2	Deviation errors of experimental results . . . . .	77
<b>F</b>	<b>Block Diagram in LabVIEW</b>	<b>79</b>
<b>G</b>	<b>A description of the OLGA base case for severe slugging.</b>	<b>81</b>
<b>H</b>	<b>Comparison of experimental and modeling results.</b>	<b>83</b>

# List of Figures

2.1	Illustration of riser slugging cycle. . . . .	6
2.2	A flowsheet of the control structure in the miniloop riser system. . . . .	8
2.3	Block diagram of a feed-back control. . . . .	8
3.1	A sketch over the miniloop. . . . .	11
3.2	Logged data from LabVIEW at liquid flow of 3 l/min and gas flow 4 l/min. . . . .	14
3.3	An illustration of how the buffer tank volume effects the experimental data, plot of P1 measurement. . . . .	14
3.4	Piping . . . . .	15
3.5	Water reservoir tank . . . . .	15
3.6	Separation tank for liquid and gas . . . . .	15
3.7	Buffer tank for air . . . . .	16
3.8	The water pump . . . . .	16
3.9	A pressure sensor . . . . .	16
3.10	Gas flow rate meter . . . . .	17
3.11	Water flow rate meter . . . . .	17
3.12	The control valve . . . . .	17
3.13	Manual gas and water valve . . . . .	18
3.14	Cabinet with the Field Point modulus . . . . .	18
3.15	Comparison of measured and real liquid flow. . . . .	20
3.16	Comparison of measured pressure in LabVIEW and real pressure. . . . .	21
3.17	Front panel in LabVIEW . . . . .	22
4.1	Logged data at liquid flow rate at 3 l/min and gas flow rate at 7 l/min, illustrating continuous flow. . . . .	25
4.2	Logged data at liquid flow rate at 3 l/min and gas flow rate at 5,5 l/min, illustrating hydrodynamic flow. . . . .	26
4.3	Logged data at liquid flow rate at 3 l/min and gas flow rate at 5 l/min, illustrating transition between hydrodynamic flow and severe slugging type I. . . . .	27
4.4	Logged data at liquid flow rate at 3 l/min and gas flow rate at 3 l/min, illustrating severe slugging type I flow regime. . . . .	28
4.5	Logged data at liquid flow rate at 12 l/min and gas flow rate at 4 l/min, illustrating severe slugging type II flow regime. . . . .	29
4.6	Logged data at liquid flow rate at 12 l/min and gas flow rate at 2 l/min, illustrating bubble flow. . . . .	30
4.7	Plots from experiment with gas flow rate at 3 l/min and liquid flow rate at 4 l/min. . . . .	32
4.8	Illustration of liquid levels during slugging. . . . .	33
4.9	Flow regime map from the open-loop experiments. . . . .	35
4.10	Amplitude plot at P3 with constant gas flow rate of 3, 4 and 5 l/min. . . . .	37

4.11	Amplitude and period plot for a constant liquid flow rate of 3 l/min. . . . .	38
5.1	Illustration of how the set point effects the stability at liquid flow rate of 4 l/min and gas flow rate 3 l/min. . . . .	42
5.2	Comparison of real P1 and filtered P1 measurements. . . . .	43
5.3	A comparison of P-control (to the left) and PD-control (to the right) at liquid velocity of 4 l/min and gas flow of 4 l/min. . . . .	44
5.4	A comparison of P-control (to the left) and PD-control (to the right) at liquid velocity of 12 l/min and gas flow of 4 l/min. . . . .	44
5.5	Results from the closed-loop experiments. . . . .	46
5.6	The effect of control on the severe slugging II region at liquid flow rate of 12 l/min and gas flow of 4 l/min. . . . .	48
5.7	Result from bifurcation map experiment with liquid flow of 4 l/min and gas flow 4 l/min. . . . .	50
6.1	Snapshot of the model of miniloop in OLGA. . . . .	54
6.2	Comparison of simulation and experimental results of severe slugging type I at flow rates of gas and liquid at 3 l/min. . . . .	55
6.3	Comparison of simulation and experimental results of severe slugging type II, for liquid flow rate at 12 l/min and gas flow rate of 4 l/min. . . . .	55
6.4	Comparison of simulation and experimental results of continuous flow. The liquid flow rate is 20 l/min and the gas flow rate 5 l/min. . . . .	56
6.5	Comparison of the pressure in the buffer tank (P3) for different gas flow rates in experiment and in OLGA. . . . .	58
6.6	Comparison of simulation and experimental results of inlet pressure with constant liquid flow of 3 l/min. . . . .	59
6.7	Comparison of simulation and experimental results of period between slugging with constant liquid flow of 3 l/min. . . . .	59
F.1	Blockdiagram in LabVIEW . . . . .	79
H.1	Table of OLGA and experimental comparisons. . . . .	84
H.2	Continued table of OLGA and experimental comparisons. . . . .	85

# List of Tables

3.1	Symbols describing the miniloop . . . . .	12
3.2	Parameters from experimental setup . . . . .	13
3.3	An overview of modifications made to the miniloop. . . . .	13
3.4	Original parameters from LabVIEW . . . . .	19
3.5	New parameters for pressure measurements in LabVIEW . . . . .	21
3.6	Logged values in LabVIEW . . . . .	22
4.1	Fallback time and slugging period for different flow rates. . . . .	33
5.1	Boundary to severe slugging type I for open-loop and closed-loop operation. . . . .	47
5.2	Comparison of frequency and inlet pressure amplitude for severe slugging type I and II. . . . .	47
5.3	Decrease in back pressure with closed-loop setup. . . . .	49
5.4	Results from bifurcation experiment . . . . .	50
B.1	Values from liquid calibration experiment. . . . .	69
B.2	Voltage for each run in liquid flow meter calibration. . . . .	70
B.3	Real pressure, pressure from LabVIEW and voltage signal from P1 calibration. . . . .	71
B.4	Real pressure, pressure from LabVIEW and voltage signal from P2 calibration. . . . .	71
B.5	Real pressure, pressure from LabVIEW and voltage signal from P3 calibration. . . . .	72
D.1	Parameters used for conversion of liquid flow . . . . .	75
D.2	Conversion of liquid volume flow to the liquid flow velocity . . . . .	76
D.3	Conversion of gas volume flow to the gas flow velocity . . . . .	76
E.1	The deviation errors during liquid calibration . . . . .	77
E.2	The deviation in liquid flow rate at different values . . . . .	78
G.1	Geometry of severe slugging base case model in OLGA. . . . .	81
G.2	Inputs to the severe slugging base case model in OLGA. . . . .	81



# Chapter 1

## Introduction

The Master's thesis is the final part of the five year Chemical Engineering education at the Norwegian University of Science and Technology (NTNU). The experiments of this project have been carried out in collaboration with postdoc student Weiwei Qiu, who will use the results as a part of her work. The thesis has been carried out at the Department of Chemical Engineering, with some contribution from the Department of Energy and Process Engineering.

### 1.1 History and previous work

Multiphase pipelines connecting the subsea wells to platforms in the North Sea have become a common feature, and the number of remote wells being connected to existing facilities will continue to increase [1][2]. A serious issue that arises with this development is unstable flow in the multiphase pipelines entering the separation facility. This flow is characterized by variations in the flow at the pipeline outlet. Control of the flow entering the separation process is referred to as flow assurance, and has become an increasingly important topic.

One form of flow variation is slug flow. This flow regime arises when "slugs" of liquid accumulate before being pushed out through the pipeline by the gas. Slug flow leads to oscillations of the pressure in the pipeline and variations in the flow rates of gas and liquid. Slugs form when the liquid blocks the low end of the pipe. The liquid flowing upstream the blockage makes the slug grow, while the gas flow contributes to a pressure build up. When the pressure is high enough, the gas will push the liquid slug up through the pipeline. The liquid and gas flow rate at the outlet increases and the pipeline is depressurized. A new slug will start to form, and the process is repeated. This regime typically becomes a problem at the tail production of an oil field [3]. The pressure in the wells is often reduced towards the end of the well lifetime, causing riser slugging [4].

Some consequences of slug flow are:

- Variation of liquid level in the separation unit can lead to poor separation and possible overflowing.[5]
- Pressure fluctuations wear and tear on the equipment and can cause unplanned shutdown periods.[5]
- Rapid variation in outlet flow rates causes unwanted flaring which increases the environmental effect of oil production. [1]
- Large and rapidly varying compressor loads which reduces the efficiency and capacity of the compressor [1]

The effects of slug flow push the operation away from the optimal point. This is why a lot of money is spent on flow assurance. By installing slug-catchers or increasing the first-stage separation unit to increase the buffer capacity, the effects of the large flow and pressure variations can be reduced. However, modifying the process design at existing facilities can be inconvenient and increases the capital costs.[1] Another method is to choke the top-side valve upstream the separator to eliminate the slugging. The flow is stabilized, but the production rate of oil decreases at the same time. This motivates the investigation of dynamic control of the valve. [3]

An approach based on feedback control was first proposed by Schmidt et. al. (19780) [6]. The concept of this paper was to suppress terrain slugging by using the top-side choke valve and a feedback control structure using both the pressure measurements at the inlet and upstream the riser as inputs. A series of experiments was conducted on a small-scale loop. These results were followed up by Hedne and Linga (1990), who used a standard PI-control of the pressure at the low-point of the riser in a medium-scale experiment. [7] Research and testing within this topic has been conducted by many people since then. Testing of different control structures have also been conducted in simulators like OLGA and Matlab (see references [8], [5], [3]), in addition to further experimental testing ( [8], [2], [9]). Several systems are now in operation offshore [7], one example is slug control installed on Heidrun in 2001[4] .

## 1.2 Scope of work

The motivation for this project is to study how a dynamic feedback controller can increase the oil production at the tail production of an oil field. When the flow rates of liquid and gas become sufficiently low, the flow regime will move toward the severe slugging region. Flow regimes at different flow rates of liquid and gas will be mapped, with and without active control. Two gains from dynamic control will be considered, increased production rate and extended production time. By assuming a constant liquid to gas ratio in the reservoir, the production rate will have a linear equation passing through the original at tail production of the field. If the criterion of production is stable flow, the gain of the controller will be the extended line before moving into a severe slugging region. There will be no economic evaluation of the end production of a reservoir in this thesis. The cost of leasing the platform versus the gain of production will not be evaluated.

This thesis can be divided into three sections. First an open-loop experiment was conducted with the miniloop. This was a two-phase flow experiment with water and air, representing oil/water and hydrocarbon gas flow from a reservoir. The goal of this experiment was to produce a flow regime map, depending on the flow rates of the water and air. Even though the values in the flow map from the miniloop can not be used directly for differently scaled systems, the results are important in the study of the dynamics of the different flow regimes.

The second part of this project was to add a P-controller and PD-controller with filter to the system, and see which points in the severe slugging region could be stabilized. Tuning of these controllers was done by trial and error. When comparing the results of the flow map, with and without active control, it can be determined what effect the controller has when the production rate decreases. A bifurcation map was produced to determine the effect of the controller on the production rate.

The last part of this thesis was to compare the experimental open-loop results with a model simulated in OLGA. The main purpose of this task was for the author of this thesis to get acquainted with the simulation language.



# Chapter 2

## Theory

### 2.1 Flow regimes in two-phase pipelines

In a multiphase flow, different flow regimes can arise, depending on flow rates, fluid properties and pipeline geometry [5]. Some flow regimes include stratified flow, annular flow, bubble flow, slug flow and churn flow [8]. Transition between the different flow patterns can also occur.

Slug flow can vary in frequency and magnitude. In this thesis, the different slugging phenomenons will be divided into four categories [8]:

- **Hydrodynamic slugging**  
Hydrodynamic slugs are initiated in the horizontal parts of the pipeline by instability of waves on the gas-liquid interface. When the velocity difference between the gas and liquid phase is large enough, the liquid wave is lifted to the top of the riser and eventually covers the whole cross section. Once the wave reaches the top of the pipe, a slug is formed. Gas pushes the slug at a greater velocity than the liquid film, and the liquid is accumulated in the slug. The turbulence within the slug increases because of gas entrainment [10]. The inlet separator will in most cases be able to handle these types of slugs [4].
- **Riser slugging**  
Riser slugging can occur in a system where a down-sloping pipeline is attached to a riser [8]. The low-point fills with liquid and blocks the gas flow. The liquid slug accumulates at the base of the riser, at the same time the pressure at the low-point builds up. This continues until the pressure is high enough to overcome the hydrostatic head and the liquid slug is pushed out of the riser [10]. The cycle repeats itself. Riser slugging will also be referred to as severe slugging in this thesis.
- **Terrain slugging**  
Terrain slugging can develop in horizontal and undulate pipelines, for example pipelines over rough seafloor terrain. Liquid accumulated in inclined sections is picked up by the slugs and can become very extensive [8].
- **Transient slugging**  
If there is a change in operating conditions, transient slugging can occur at the exit of the

pipeline [8]. Change in flow rates and pressure are examples of operating conditions that can induce transient slugging. This is a typical problem during start-up and shut-down [10].

In an oil/water-dominated system, the riser slugging will have the most serious consequences [8]. Severe slugging is characterized by liquid slugs ranging in length from one to several riser heights depending on the pipeline geometry [11]. This flow regime is considered to be an "unstable" flow regime because it is associated with large fluctuations in the pipeline pressure and the outlet flow rates [12]. Figure 2.1 illustrates how the riser slugging cycle can be divided into four steps.

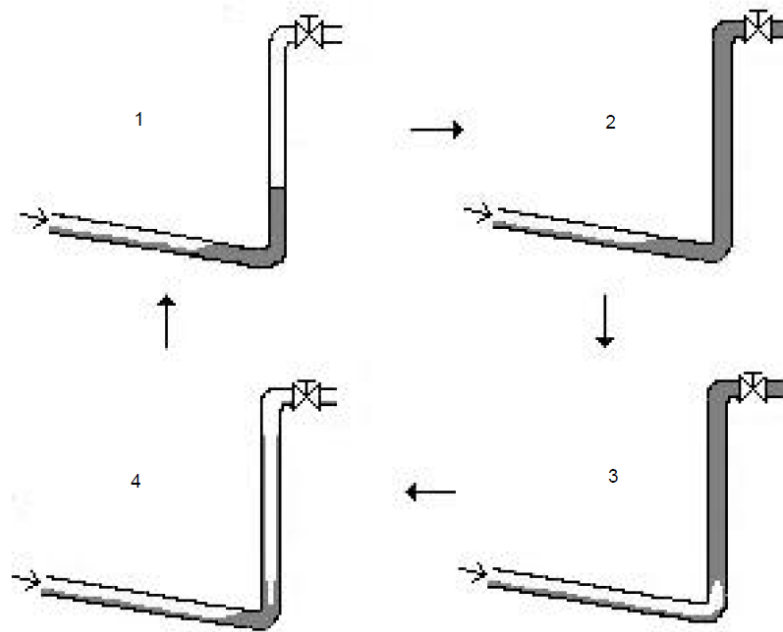


Figure 2.1: Illustration of riser slugging cycle. [5]

First the liquid accumulates at the low point of the riser (step 1), blocking the gas flow. It is the gravity of the liquid that causes this phenomenon. If the flow rates are sufficiently high, the liquid flow is able to overcome the gravitational force. Gas and liquid is continuously entering the system, causing the slug in the riser and the pressure upstream the slug to grow (step 2). When the pressure build up overcomes the hydrostatic head of the liquid, the gas will start to penetrate the liquid and blow the slug out of the riser. At the same time, the gas will expand and increase the flow velocities (step 3). After the blow out, the gas velocity is no longer high enough to drag the liquid upwards. The liquid will start to fall back down in the riser and a new slug will start to accumulate (step 4).

### 2.1.1 Severe slugging definitions

The severe slugging flow regime can be divided into groups depending on the characteristics of the flow regime. There exist different definitions on the severe slugging types. Schmidt et. al. [12][11], differentiated between slugging type I and II. In type I slugging the slug length should

exceed the riser length and appears at lower liquid and gas velocities. The characteristics of type II slugging flow pattern is similar to the type I except the liquid slugs are slightly aerated and the slug lengths do not exceed the riser height. Increasing the gas flow rate beyond the type II region, the gas upstream the riser will start to penetrate the liquid slug and separate the slugs by bubbles. This region is termed "transition to severe slugging".

Taitel et. al. [13] described severe slugging with no gas penetration by the definition of Schmidt et. al. In addition, the quasi-steady process of gas penetration is divided into three different flow configurations (the region Schmidt et. al. defined as "transition to severe slugging"):

1. Riser oscillation, ending in a stable steady state two-phase flow
2. Cyclic operation without fallback
3. Cyclic operation with fallback

Both processes 2 and 3 are severe slugging cycles. In process 2 the liquid flow velocity is high enough to carry the liquid slug out of the riser, while in process 3 the liquid will fall down due to lower liquid flow rates. After the fall down the liquid will propagate up the riser.

In this thesis the severe slugging will be divided into type I and type II. The type I slugging will be used for flow patterns defined as type I by Schmidt et. al [11]. This type of slugging is identified with long time periods between each slug and large pressure amplitudes. The frequency and amplitude of the pressure measurements are constant when the gas and liquid flow rate remain unchanged. Type II in this thesis is the flow pattern "cyclic operation without fallback" by Taitel et. al [13]. In this region the slugs appear more frequent, and the amplitude of the pressure variations decrease. Small gas bubbles are able to escape the liquid blockage while the riser is filled with liquid. Transition state in this thesis is defined as the transition between continuous flow and severe slugging. This includes hydrodynamic slugging and an alternating hydrodynamic and severe slugs.

Bubble flow exists at high liquid flow rates and low gas flow rates. This flow regime is identified with continuous bubble flow in the riser. There is no liquid blockage the low point of the riser as the gas entering the system forms bubbles directly and are transported up through the riser with the liquid. The pressure at the inlet is close to constant.

## 2.2 Control

The control structure used in this thesis involves the feedback controller. This control system is based on that the controller responds when the controlled variable moves away from the setpoint. It is not able to act before the incident occurs. A flowsheet of the feedback control structure in the riser system and the corresponding block diagram is given in figures 2.2 and 2.3 respectively. The dotted lines in the flowsheet (figure 2.2) are electrical signals. PT is the pressure transmitter and PC the pressure controller.

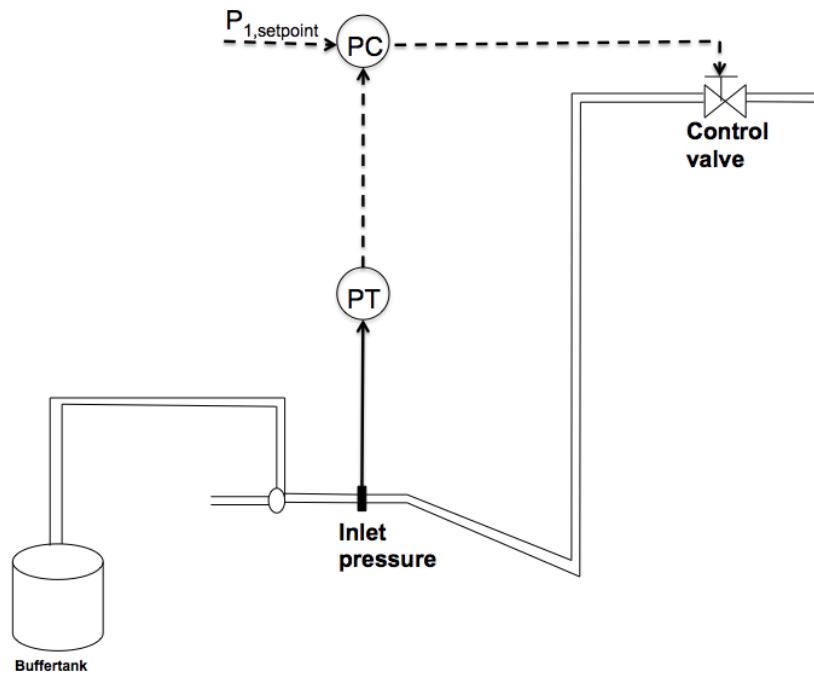


Figure 2.2: A flowsheet of the control structure in the miniloop riser system.

The variables in figure 2.3 are:

- $y_{SP}(t)$  is the set point value
- $y(t)$  is the measured value from the plant
- $e(t)$  is the error,  $e(t) = y_{SP}(t) - y(t)$
- $u(t)$  input to the plant

In LabVIEW, the controller is a PID controller in parallel. The output from the controller is given by the equation 2.1.[14]

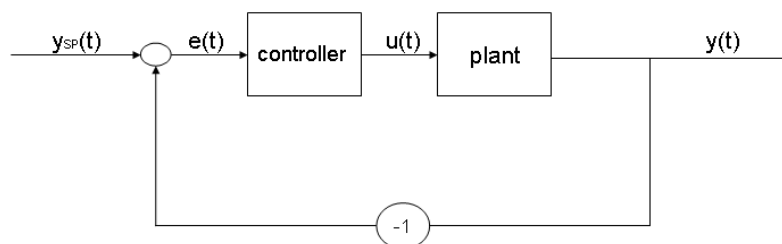


Figure 2.3: Block diagram of a feed-back control.

$$u(t) = \bar{u} + K_C \left[ e(t) + \frac{1}{\tau_I} \int_0^t e(t^*) dt^* + \tau_D \frac{de(t)}{dt} \right] \quad (2.1)$$

In this equation, the first term is the bias. As long as the error is zero, the controller output is equal to the bias. Inside the bracket, the first term is the proportional control, the second term the integral action and the last term the derivative control. The three controllers considered in this thesis are [14]:

- P-control

This proportional controller consists of the bias and the first term in the bracket of equation 2.1:  $u(t) = \bar{u} + K_C e(t)$ . The controller gain ( $K_C$ ) is used to adjust the sensitivity of the controller to the error, and determine the controller action when the error varies by setting the sign of  $K_C$ . One problem with the proportional controller is the offset. The offset is the steady-state error. To eliminate the offset after a step or disturbance occurs, the set point or the bias must be manually adjusted. If an offset is tolerated, the proportional controller is preferred because of its simplicity.

- PI-control

The PI controller consists of the bias term, the proportional and integral action:

$u(t) = \bar{u} + K_C e(t) + K_C \frac{1}{\tau_I} \int_0^t e(t^*) dt^*$ .  $\tau_I$  is referred to as the integral time, and can be thought of as the time for the integral action to take place or the time for the integral action to repeat itself. The  $\tau_I$  makes the integral action inefficient against sudden deviations in the output because the corrective action depends on the duration of the deviation. If  $\tau_I$  is too high, the integral action is eliminated because  $\frac{1}{\tau_I}$  moves towards zero.

The advantage of the PI-controller is that the offset is eliminated. At the same time, the integral action can produce oscillatory responses and reduce the stability region of a feedback controller. Another phenomenon is integral windup. This situation occurs when the error increases rapidly and the integral term becomes so large that the controller output saturates. Integral windup is when the integral term increases further while the controller is saturated.

- PD-control

The equation for this controller is given by:  $u(t) = \bar{u} + K_C e(t) + \tau_D \frac{de(t)}{dt}$ . This controller has the advantage that it can predict the future behavior of the error deviation by considering the rate of change ( $\frac{de(t)}{dt}$ ). The derivative action is zero as long as the error is constant, this is why the derivative term is never used alone.

The derivative action tends to stabilize the controller. It lifts the phase and increases the stability region. Another advantage is that the derivative mode decreases the settling time of the process, which is the time it takes for the process to reach steady-state.

When applying the derivative action to a process, it is important to be aware of noise. Noise is high frequency, random fluctuations in the measurement output. If these measurements are not filtered, the derivative action will amplify the fluctuations. The transfer function for a filter is given by the following equation:  $g_F = \frac{1}{\tau_F s + 1}$ .  $\tau_F$  is the filter time constant, and has a value of 0.05 to 0.2 of  $\tau_D$ . The filter removes the derivative terms sensitivity to noise.

When using the P-controller in the experiment, the set point parameter ( $y_{SP}(t)$ ) was used to adjust the bias in addition to being the physical set point value. The set point is divided into

the bias and physical term:  $y_{SP}(t) = y_{SP,BIAS}(t) + y_{SP,PHYS}(t)$ . This gives the output from the controller on the form:

$$u(t) = \bar{u} + K_C y_{SP,BIAS}(t) + K_C (y_{SP,PHYS}(t) - y(t))$$

If the bias value is too low, the set point parameter will be adjusted to a higher value than the physical set point would be.

## 2.3 Anti-slug control

The most common method of avoiding slugging is choking the valve at the top of the riser. When decreasing the valve opening, the pressure upstream the valve will increase. At a certain critical valve opening ( $Z_{CRIT}$ ), the pressure upstream reaches a value where slugs no longer are formed [8]. At this point the pressure at the bottom of the riser is high enough to continuously penetrate the liquid in the riser. Although the flow is stabilized, choking the valve at the top of the riser decreases the production rate by increasing the liquid holdup upstream the valve, which motivates the investigation of dynamic control [3].

The well pressure is often reduced towards the end of the well lifetime. By applying dynamic control, the well lifetime can be prolonged and the production can be increased when the topside choking is minimized. [4]

The application of the feedback controller is important because it allows for operation with conditions that would otherwise not be possible. Controlling the severe slugging flow regime is a challenge because both RHP-poles and RHP-zeros are present [5]. There are some conditions where the choke valve can not stabilize the severe slugging.

# Chapter 3

## Experimental setup

A small scale two-phase flow loop was set up to study the dynamics of different flow regimes in riser systems. The phases consisted of water and air. An illustration of the experimental setup is shown in figure 3.1. This setup will be referred to as the miniloop throughout this thesis.

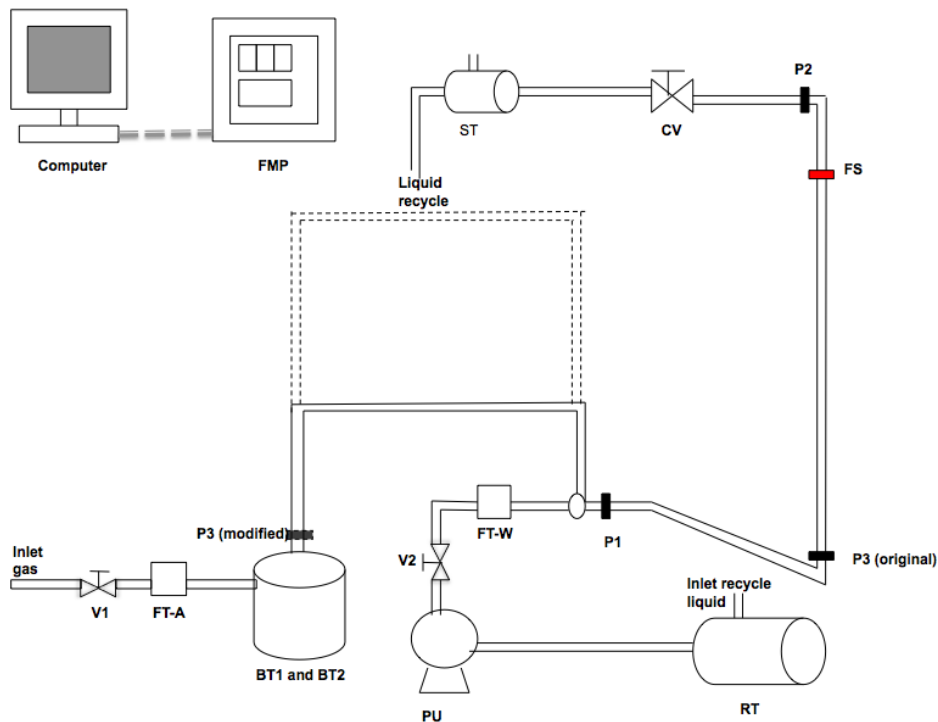


Figure 3.1: A sketch over the miniloop.

The two phases were mixed at the inlet and flowed through the low point of the system where slugging could occur depending on the conditions. At the top of the riser the water and air were separated. The air was flashed out of the system, while the liquid was recycled back to the reservoir tank. From here the water could be pumped back into the system. In order to achieve slugging, there had to be enough air in the system to blow the water out of the riser. Two

buffer tanks were placed upstream of the mixing point to attain a sufficiently high pressure build-up. The flow rate of air and water were adjusted by the valves V1 and V2. The measurement transmitters for the flow rates were placed before the mixing point. Three pressure sensors were placed throughout the system. P1 was located at the inlet, P2 at the top of the riser and P3 measured the pressure at the low point of the riser. A fiber optic sensor was placed near the top of the riser. The control valve was placed upstream the separator. This valve received signals from the control panel, determining the valve-opening.

After studying some logged data from the miniloop, inconsistencies were discovered in the results, especially when the gas flow rate was low. This was caused by water flowing into the buffer tanks and changing the gas volume in the tanks. To prevent this from happening, the tube from the mixing point to the tanks was elongated and raised to a higher elevation. This is illustrated by the dotted pipe in figure 3.1. When modifying the miniloop, the riser pipeline was replaced so that all pipeline diameters were equal. The P3 pressure sensor was moved from the low point of the riser (P3 (original) in figure 3.1) to the buffer tanks (P3 (modified)).

All the measurement signals were sent to an electrical cabinet containing the Field Point modules. This FP modules had both an input and an output module. The input module received measured signals from the system, and the output module sent signals to the control valve. LabVIEW software was used for logging and control.

A list over symbols used to describe the miniloop is given in table 3.1, with a short description.

Table 3.1: Symbols describing the miniloop

<b>Symbol</b>	<b>Description</b>
FT-W	Flow transmitter for water
FT-A	Flow transmitter for air
P1	Pressure sensor at inlet
P2	Pressure sensor at the top of the riser
P3	Pressure sensor for the buffer tanks
FS	Fiber optic sensor (slug-sensor)
V1	Manual valve for air
V2	Manual valve for water
CV	Control valve at the top of the riser
BT1	Buffer tank 1
BT2	Buffer tank 2
RT	Reservoir tank for water
ST	Separator tank at the top of the riser
FPM	Field Point Modulus

Some important parameters for the riser system is given in table 3.2

Table 3.2: Parameters from experimental setup

Parameter	Symbol	Value	Unit
Inner pipe diameter	$D_P$	20	mm
Height riser	$H_R$	3.21	m
Length of horizontal pipe from mixing point	$L_P$	0.24	m
Length of inclined section	$L_{Incl}$	2.26	m
Angle between riser and inclined pipe	$\alpha$	77.3	Deg.
Length of horizontal pipe at top of riser	$L_T$	0.13	m
Volume buffer tank	$V_B$	0.0215	m <sup>3</sup>

### 3.1 Comparison of results before and after modifications

As mentioned above, some modifications were made on the miniloop. These modifications are listed in table 3.3.

Table 3.3: An overview of modifications made to the miniloop.

Parameter	Original loop	Modified loop
Inner diameter, riser	0.018 m	0.020 m
P <sub>3</sub> sensor placement	Low point, riser	Buffer tanks
Height of pipe from buffer tank to inlet	0 m	3.21 m

In this section, plots from both experiments will be presented to show how the flow pattern changed.

Comparing the results from the original miniloop setup to the modified setup in figure 3.2, a difference in the pressure and flow rate can be observed. The period for the slugging decreased after the modifications, but this was caused by a slightly higher gas flow rate in the modified experiment. Studying the pressure measurements from the original experiment, the pressure at P1 has a peak before it decreases again. This can be explained by a small blowout of the liquid between the inlet and the buffer tank, the phenomenon disappeared after the modifications. The amplitude of the inlet pressure remained unchanged after the modifications because it depends on the liquid slug in the riser, and the height of the riser was not modified.

When the liquid was flowing into the buffer tanks, these tanks had to be continuously emptied and the respective amount of water had to be added back into the system. Figure 3.3 below illustrates a severe case of experimental error that can occur when gas volume in the buffer tanks change.

Liquid is flowing into the buffer tank during the pressure build up in the first slug (the first 50 seconds). This decreased the buffer capacity, and it took a shorter time for the pressure to reach the same height in the next slugging cycle. After 200 seconds the buffer tank was emptied. The buffer volume and the time to reach the blow out pressure in the buffer tank increased.

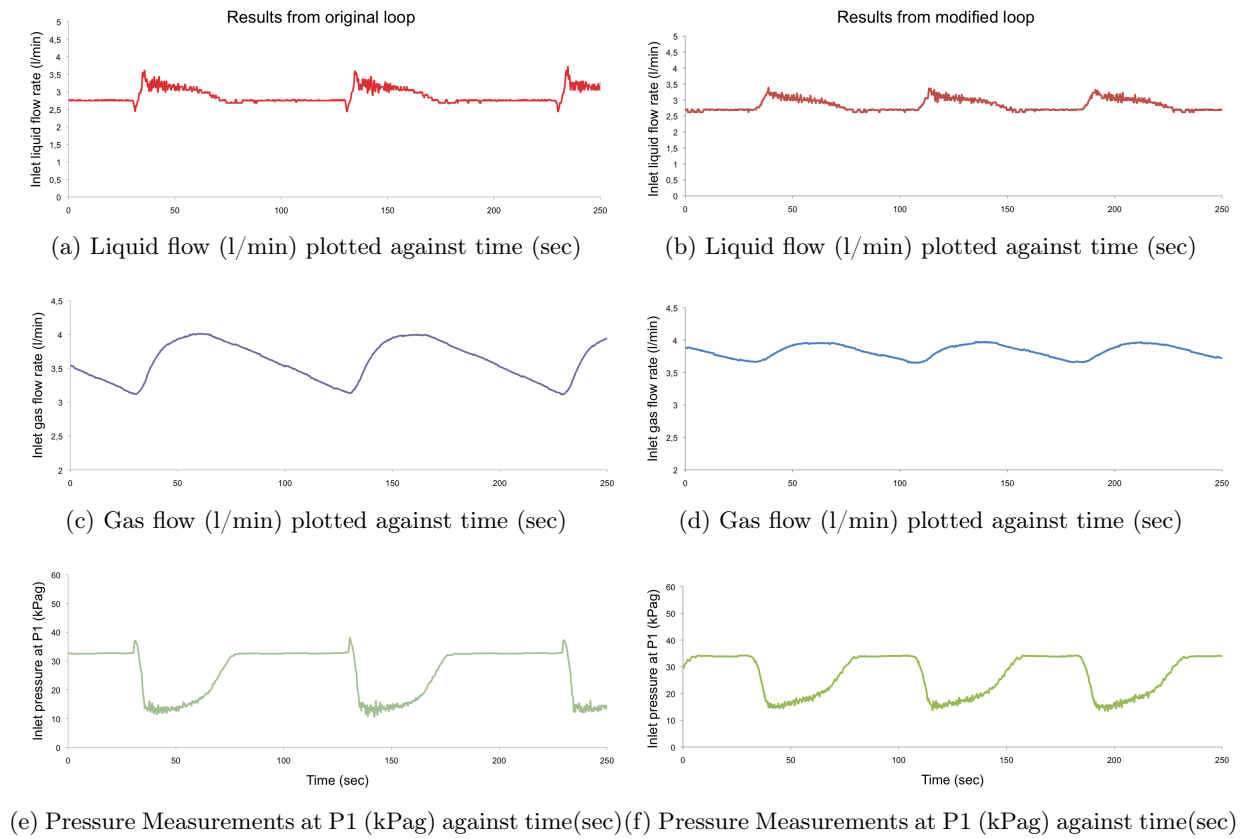


Figure 3.2: Logged data from LabVIEW at liquid flow of 3 l/min and gas flow 4 l/min.

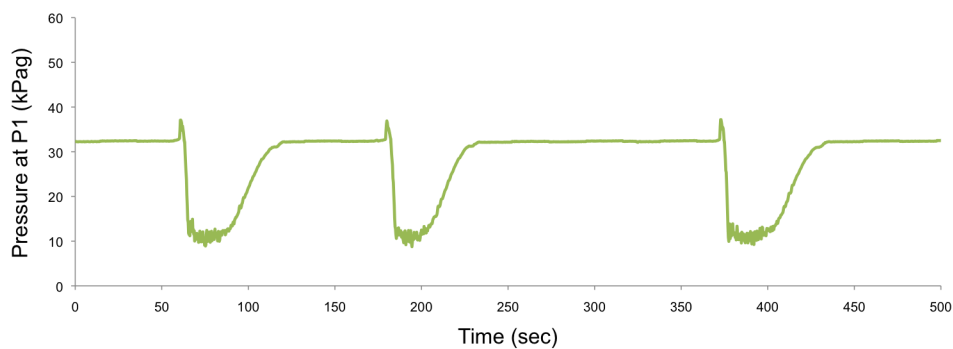


Figure 3.3: An illustration of how the buffer tank volume effects the experimental data, plot of P1 measurement.

## 3.2 Equipment

This section will give a short description and photos of the equipment used in the experiment.

A small segment of the piping is illustrated in figure 3.4. The pipes used in the miniloop had an inner diameter of 20 mm and were made of transparent silicon-rubber.



Figure 3.4: Piping

The water reservoir tank provided the capacity to maintain a continuous feed of liquid to the system. The feed to the tank came from the separation unit. It was important that the liquid level in the tank was above the outlet opening to avoid gas entering the pump. The reservoir tank was made of see-through plexiglas, and had a cylindrical shape. A picture of the water tank is shown in figure 3.5



Figure 3.5: Water reservoir tank

The separator tank was situated at the top of the riser, downstream the control valve. The gas phase was released to the environment from the top of the separator and the liquid phase was recycled back to the reservoir tank. Figure 3.6 shows the separator unit, it had a cylindrical shape and was made out of transparent plexiglas.

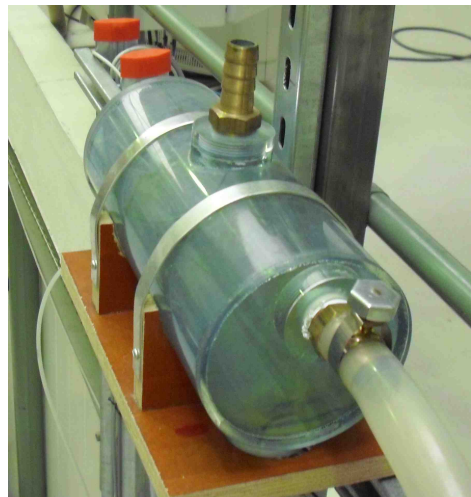


Figure 3.6: Separation tank for liquid and gas

Two buffer tanks for air were connected with a large diameter pipe to provide a sufficiently large volume for pressure build up during slugging. Both tanks were cylindrical and were situated between the air inlet and the mixing point for liquid and gas. The buffer tanks had a safety valve that opened if the pressure reached a certain critical level. These tanks were also made of see-through plexiglas. The volume available for air could be adjusted by disconnecting one of the tanks or partly filling them with water. Figure 3.7 illustrates the smallest of the buffer tanks, the larger tank is can be seen in the background.



Figure 3.7: Buffer tank for air

The water pump is shown in figure 3.8. It was placed between the water reservoir tank and the mixing point of liquid and gas.



Figure 3.8: The water pump

Three pressure sensors were located at different places in the miniloop, named P1, P2 and P3. They measured the pressure difference between the atmosphere and the pipe. The measurements were sent to the FP-modulus as analogue voltage signals. The measured values illustrated in LabVIEW had the unit kPag. Figure 3.9 illustrates one of the pressure sensors.



Figure 3.9: A pressure sensor

The flow rate meter for air was placed upstream the buffer tanks. The flow rate was given in l/min on the display. It had a range of 0 - 10 l/min. The signals were sent to the FP-modulus with an analogue 0-5 V signal. Figure 3.10 shows the flow rate meter for air.



Figure 3.10: Gas flow rate meter

The flow rate meter for water was located upstream the mixing point. It was based on a turbine flow measurement [2]. This flow meter also displayed the flow rate in l/min. The signals sent to the FP-modulus were 4-20 mA analogue current signals. This flow meter is depicted in figure 3.11.



Figure 3.11: Water flow rate meter

The control valve was located at the top of the riser, upstream the separator. It received signals from the FP-module, where signals between 0-10.2 V were converted to a current signal using a linear relationship. The control valve is depicted in figure 3.12.



Figure 3.12: The control valve

The air and water flow rate were manually adjusted by the valves in figure 3.13. The valve on top is the gas valve and the picture below the liquid valve. These were placed upstream the mixing point of the two phases.

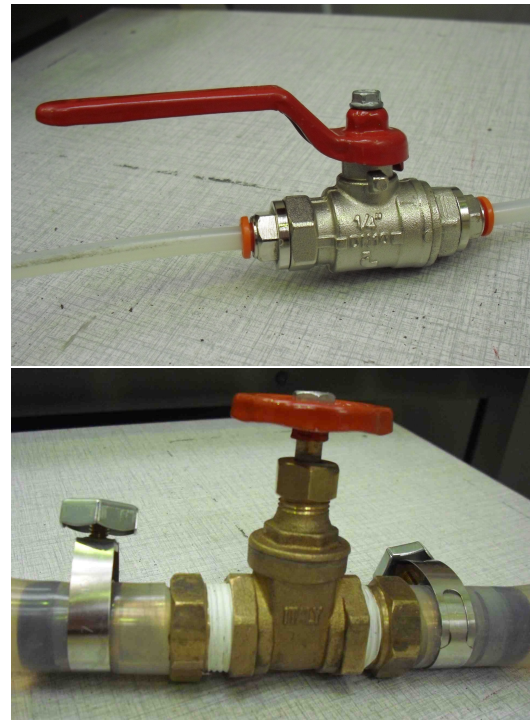


Figure 3.13: Manual gas and water valve

The Field Point modulus was necessary for logging and saving the measurements during the experiment. The FP-modulus had an Analogue Input (AI) and an Analogue Output (AO) modulus. The AI received data from all measurement instruments, while the AO section was connected to the control valve. Each of these modulus' could be connected to maximum 8 instruments each. A FP-driver was needed to transfer the data from the FP-modulus to a software on the computer. The driver used was National Instruments's "Measurement & Automation Explorer, version 4.1" connected to the computer with LabVIEW software. Figure 3.14 shows the FP-modulus inside a waterproof cabinet. [2]

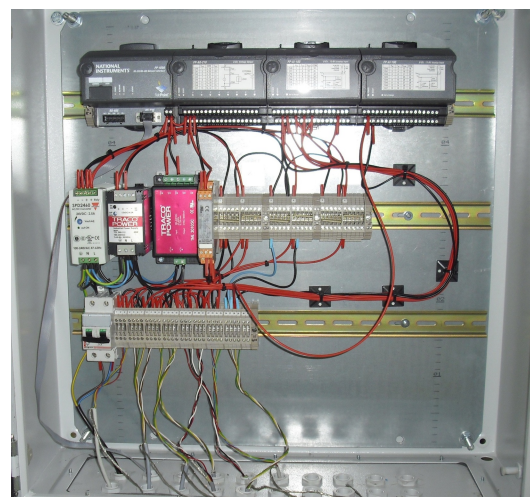


Figure 3.14: Cabinet with the Field Point modulus

### 3.3 Calibration of equipment

Before starting the experiments, a test-run on the original miniloop was conducted to get an overview of the system. It was discovered that the pressure measurement at point P1 was larger than at the point P3 in the original setup. Point P3 was at a lower elevation than P1, and the pressure should increase when the elevation decreases. The liquid flow meter was calibrated at the same time to be certain that it showed the correct value.

The measured values in LabVIEW were linear functions of voltage coming from the measurement apparatus. When conducting the calibration, these functions were examined. The linear equation was expressed as follows:

$$y = mx + b \quad (3.1)$$

Here  $y$  was the measured variable and  $x$  was the voltage from the apparatus.

The liquid flow meter was calibrated by filling a bucket of water, weighing the contents and taking the time to fill it. The values calculated from these tests represented the real liquid velocity. The raw data from the calibration is given in appendix A and the calculations are shown in appendix B.1. It was assumed a water density of  $1000 \text{ kg/m}^3$  during the calculations.

The pressure measurements were calibrated by closing the miniloop. When no liquid or gas entering or leaving the system, the pressure should be equal at all the measuring points. A pressure calibrator was added to the loop. With this apparatus the closed loop pressure could be adjusted and measured accurately.

The original parameters for equation 3.1 in LabVIEW were:

Table 3.4: Original parameters from LabVIEW

<b>Liquid flow</b>	
m	3738.90
b	-14.96
<b>Pressure</b>	
m	23.26
b	-4.65

The three pressure measurements were adjusted by the same parameters of  $m$  and  $b$ .

#### Liquid flow calibration

By rewriting equation 3.1 to the form  $x = (y - b)/m$  and using the measured values in LabVIEW ( $y$ ) and the original parameters in table 3.4, the voltage at each liquid velocity could be found. Figure 3.15 shows the difference in the real and measured liquid velocity. Results are given in appendix B.2.

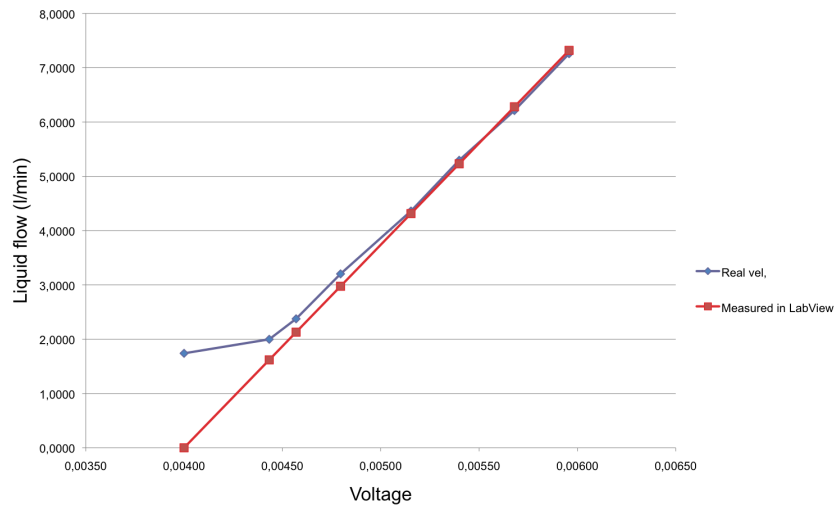


Figure 3.15: Comparison of measured and real liquid flow.

It is clear from this plot that the liquid flow meter was less accurate at low liquid velocities. Below 1.6 l/min the flow meter jumped to zero. The first point of the real liquid flow plot is also incorrect, because the voltage at this point was unknown.

When comparing the linear equation for the real liquid flow above 1.6 l/min, the parameters are almost the same at the original parameters. The equation for the liquid flow measurement in LabView was not changed.

The second flowmeter that was added to the miniloop to measure the lower flow rates, was calibrated in the same manner as the original flowmeter. Comparing the results from the filling the bucket and the measured values, the difference was small.

### Pressure calibration

The procedure to find the voltage from each of the pressure measurements was the same as in liquid calibration. The results from the pressure calibration is shown in figure 3.16. The values for the pressure calibration plots are given in appendix B.3.

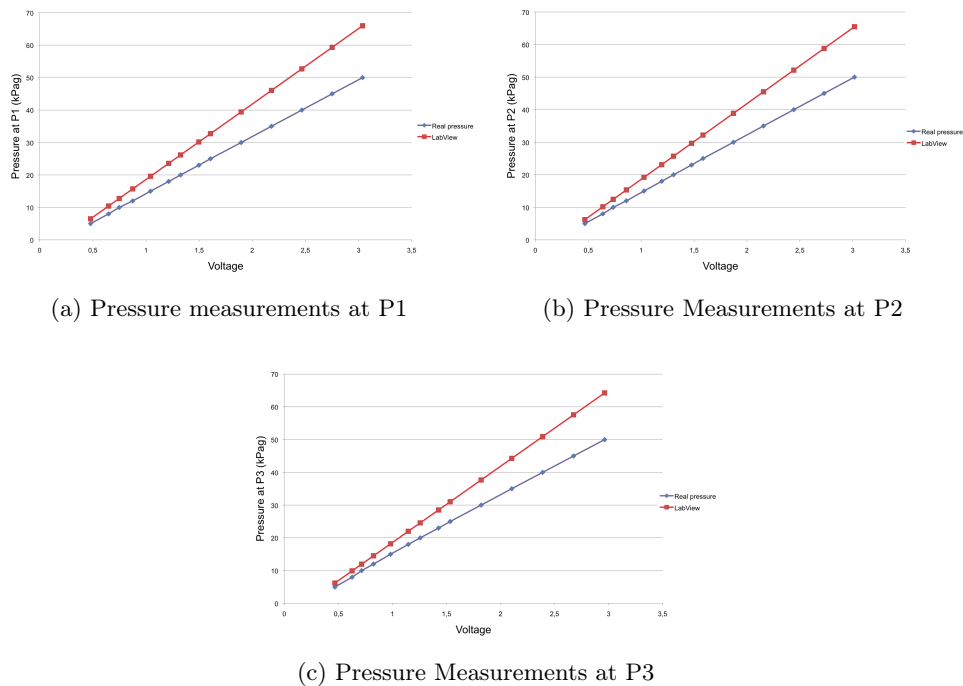


Figure 3.16: Comparison of measured pressure in LabVIEW and real pressure.

The blue line indicates the real pressure at the different voltages, while the red line is the pressure from LabVIEW. To find the new equations for LabVIEW, the linear trendline function in Excel was used. The new parameters for the equations in LabVIEW were:

Table 3.5: New parameters for pressure measurements in LabVIEW

	<b>P1</b>	<b>P2</b>	<b>P3</b>
m	17,57	17,65	17,94
b	-3,31	-3,11	-2,82

### 3.4 LabVIEW

LabVIEW is short for Laboratory Virtual Instrumentation Engineering Workbench, and was created by the National Instruments Corporation (Austin, Texas) over twenty years ago. The programming language is called G and is based on C+ [2]. This program can be divided in to two separate parts, the front panel and the block diagram. Figure 3.17 illustrates the front panel for the miniloop experiment.

The values plotted in the front panel are: pressure at P1, P2 and P3, voltage from the slug sensor, the volumetric flow rate of water and air, the set point value for controlled variable and the position of the valve opening. In the top left corner of figure 3.17, the position of the valve opening is shown and the controller parameters right below. The controller was switched on

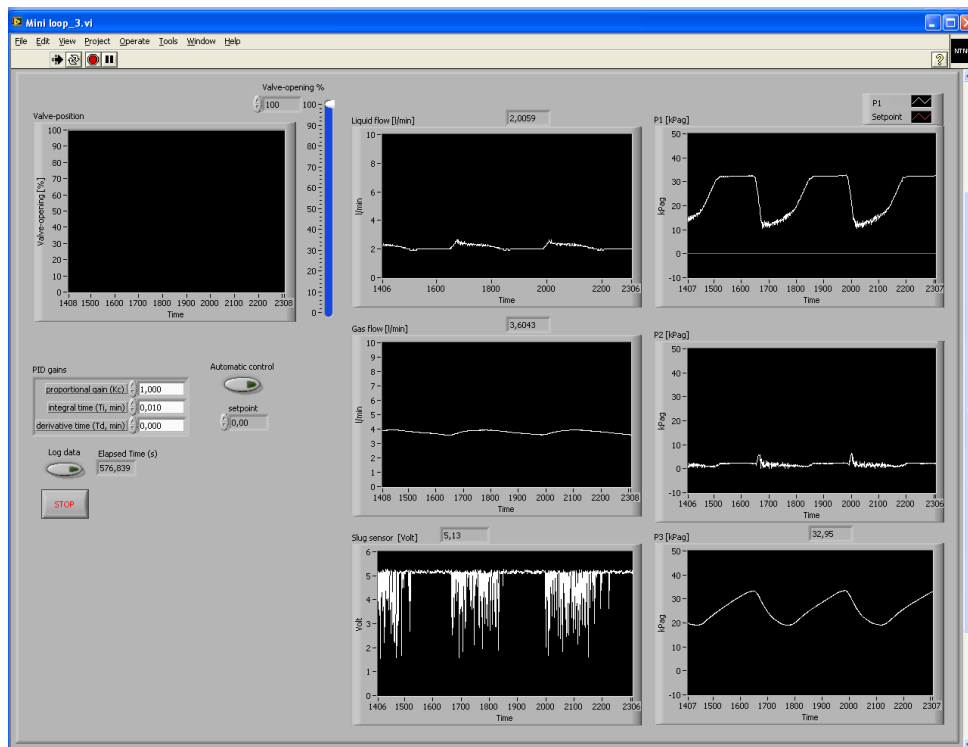


Figure 3.17: Front panel in LabVIEW

with the "Automatic Control" button. When the controller was not activated, the valve opening could be manually adjusted by typing in the preferred value in the box above the valve opening screen. The values logged from LabVIEW are illustrated in table 3.6

Table 3.6: Logged values in LabVIEW

t (sec)	$Q_G$ (l/min)	$Q_L$ (l/min)	P1 (kPag)	P3 (kPag)	P2 (kPag)	SP (kPag)	S (V)	Z (%)
...	...	...	...	...	...	...	...	...
...	...	...	...	...	...	...	...	...

All programming is done using block diagrams consisting of icons and wires, this diagram was ready for use when the experiments for this thesis started. A section of the block diagram for this experiment is illustrated in appendix F.

## Chapter 4

# Open-loop experiment

This section describes the experiments carried out with the control valve (CV in figure 3.1) in manual mode and 100% open. The flow regime map from both the original and modified miniloop will be presented, while all other results are from the modified setup.

### 4.1 Experimental

The first experiment on the miniloop was to construct a flow regime map, illustrating the different flow regimes with varying gas and liquid flow rates. The procedure for this experiment was to first set the liquid flow rate to the desired value and decreasing the gas flow rate from a sufficiently high value. With this procedure, the flow regime moved from a continuous flow regime to severe slugging. The inlet liquid and gas flow rate and the pressures P1, P2 and P3 were logged from LabVIEW at each point in the flow map.

The flow regime map was first plotted using the original setup (see section 3). After discovering that there were inconsistencies in the data because of liquid accumulation in the buffer tank, the whole experiment was repeated using the modified setup described in section 3. When running the miniloop with the original setup, the buffer tanks needed to be drained from time to time. It was important to add the respective amount of water back into the system. If the liquid level in the reservoir tank became too low, gas would enter the pump and the experiment had to be stopped to remove the gas bubbles upstream the mixing point.

Because the original flowmeter was not able to measure values below 1.6 l/min, a second flowmeter was placed upstream the first one. The new flowmeter had a measurement range from 0.27 l/min to 2.5 l/min. It could not be connected to the FP-modulus, so the measurements had to be read directly from the device. This proved to be inefficient because the measured values were fluctuating too much to read of an average value.

## 4.2 Results and discussion

All the logged data during this experiment is enclosed in appendix A.

### 4.2.1 Different flow regimes

All the data recorded in LabVIEW was logged for each point in the flow regime map. When plotting the inlet pressure, liquid flow and gas flow, the flow regime could easily be identified by comparing the plots to the flow behavior in the miniloop. The pressure was logged in the unit kilopascal gauge (kPag) and the flow rates in liters per minute (l/min). In this section the plots of six flow regimes relevant for this experiment will be illustrated; continuous flow, hydrodynamic flow, transition state, severe slugging type I and type II and bubble flow.

To make the figures easy to compare and the difference in the variations clear, the same unit step in the y-axis has been used for the different plots. The pressure measurement is illustrated with an y-axis from 0-60 kPag for all the figures. The gas flow rate has a range of 2,5 l/min and the liquid flow rate a range of 5 l/min. Even though the starting value of the y-axis in the flow rate plots vary, the difference in amplitude is easy to compare because the unit steps are equal. The x-axis is the time in seconds, and is set to 250 seconds for all the plots.

When the flow regime was continuous, there were no big variations in the flow rates or pressure over time. The liquid and gas flow was continuous throughout the system. This flow regime was typical either when the liquid flow rate was high enough to pull the gas up through the riser, or when the gas flow rate was high enough to push through the liquid. Figure 4.1 illustrates continuous flow at low liquid- and high gas flow rate.

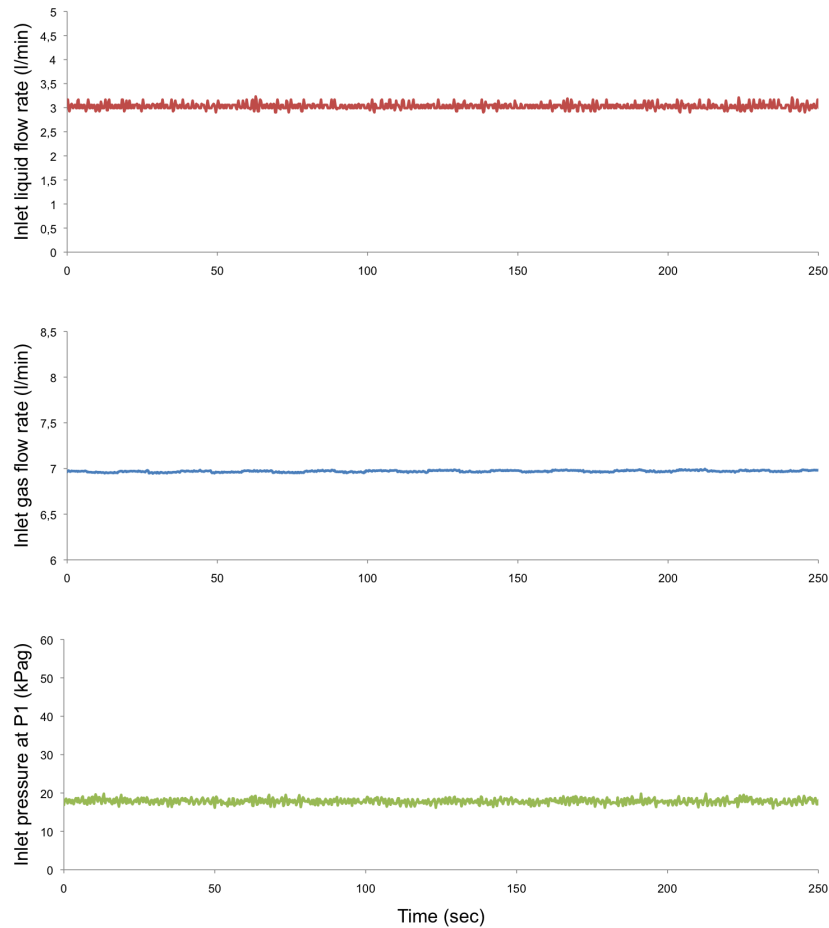


Figure 4.1: Logged data at liquid flow rate at 3 l/min and gas flow rate at 7 l/min, illustrating continuous flow.

The red plot is the water flow rate, the blue plot the flow rate for air and the green plot is the pressure measurements at P1, which is the pressure at the inlet. This color coordination will be the same for all the flow regime plots.

When keeping the liquid flow rate constant and decreasing the gas flow rate the flow regime moved towards a transition state and further into the severe slugging region. Hydrodynamic slugging is labeled as a transition state between continuous flow and severe slugging in this thesis. This flow regime is initiated in the horizontal part of the system (see section 2.1). Figure 4.2 shows how this flow regime introduced small pressure oscillations at the inlet, while the flow rates of liquid and gas were close to continuous.

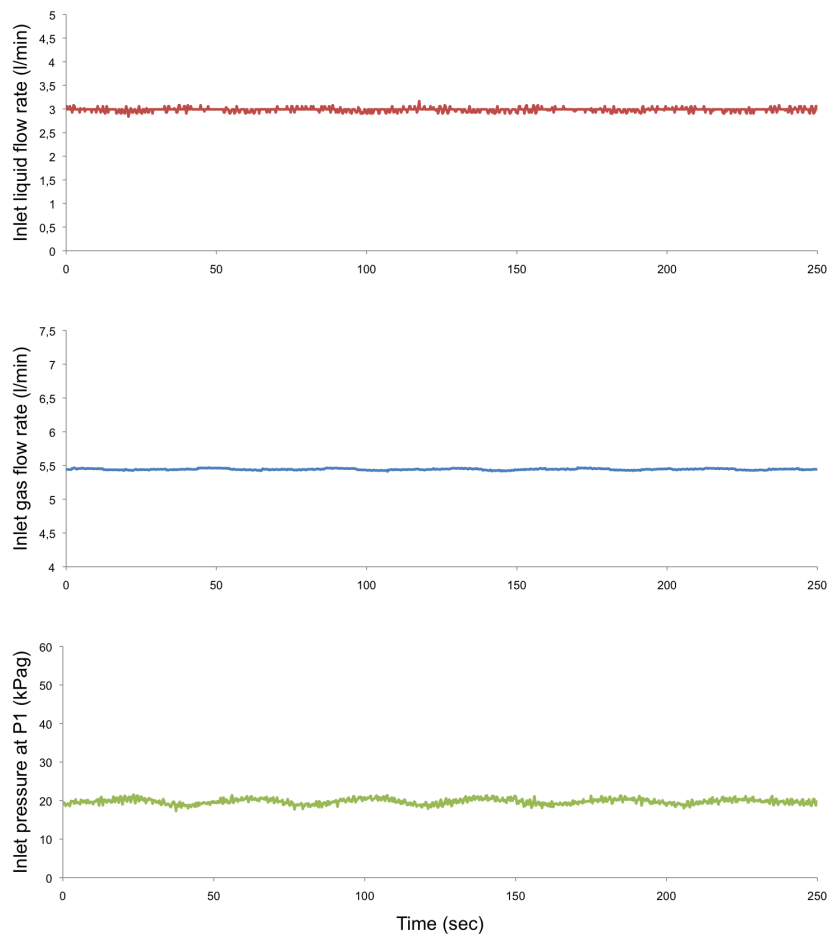


Figure 4.2: Logged data at liquid flow rate at 3 l/min and gas flow rate at 5,5 l/min, illustrating hydrodynamic flow.

When decreasing the gas flow rate slightly from this state, there was a noticeable difference in the pressure oscillations. At this combination of water and air flow rate, the pressure varied from 17 - 21 kPag.

Before entering the severe slugging region, there was a transition state between hydrodynamic and severe slugging. This is illustrated in figure 4.3. Because the liquid flow rate was low, the severe slugging in this region was of type I. The flow regime cycle consisted of a small hydrodynamic slug before a large riser slug appeared. Notice that that the change in the gas flow rate from figure 4.2 to 4.3 was only 0.5 l/min, indicating that the combination of liquid flow rate of 3 l/min and gas flow rate of 5 l/min was a boundary for the severe slugging region.

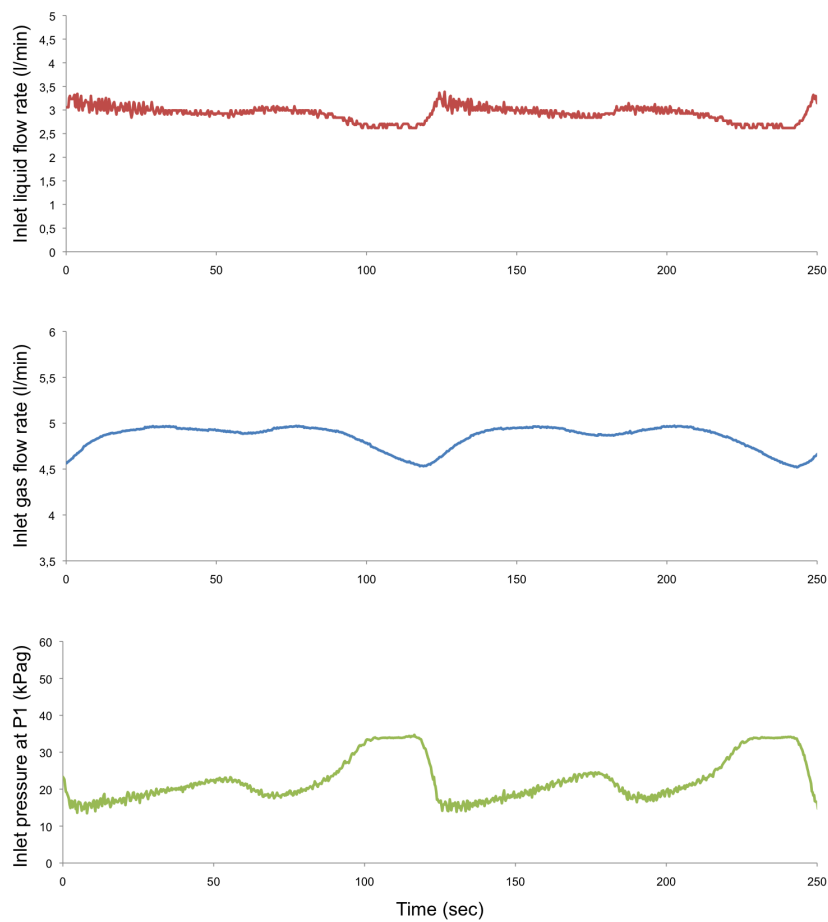


Figure 4.3: Logged data at liquid flow rate at 3 l/min and gas flow rate at 5 l/min, illustrating transition between hydrodynamic flow and severe slugging type I.

Figure 4.4 illustrates the flow regime when the liquid flow was 3 l/min and the gas flow 3 l/min. This represents a severe slugging I flow regime.

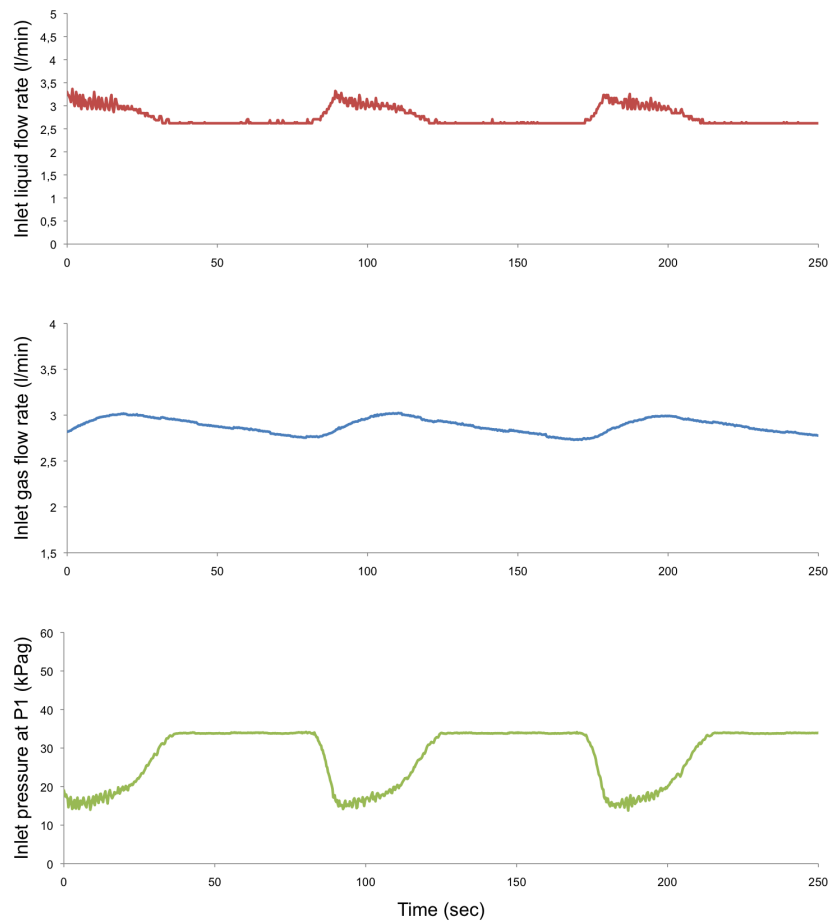


Figure 4.4: Logged data at liquid flow rate at 3 l/min and gas flow rate at 3 l/min, illustrating severe slugging type I flow regime.

Figure 4.4 clearly illustrates how the liquid and gas flow rates varied with the slugging. The slug in the riser was building up when the liquid and gas flow decreased. The liquid blocked the gas flow at the bottom of the riser, and the pressure was built up. When the pressure drop over the riser was high enough to overcome the hydrostatic head, the gas started to penetrate the liquid and pushed the liquid out of the riser. Figure 4.4 shows how the gas and liquid flow increased when it was pushed out of the riser, and the pressure upstream the riser decreased.

Decreasing the gas flow rate even further, the time to build up a high enough pressure at the bottom of the riser increased. The amplitude of the pressure variance remained almost constant, but the period between each slug increased. Decreasing the gas flow rate from 3 l/min to 2 l/min while keeping the water flow rate constant, the period between the slugs increased from 89 to 136 seconds.

When the liquid velocity was high, the flow regime moved towards a severe slugging II region, as described in section 2.1. In this region gas bubbles were continuously penetrating the liquid column in the riser, creating a cyclic behavior. Figure 4.5 illustrates a severe slugging II region. Here the liquid flow was 12 l/min and the gas flow 4 l/min.

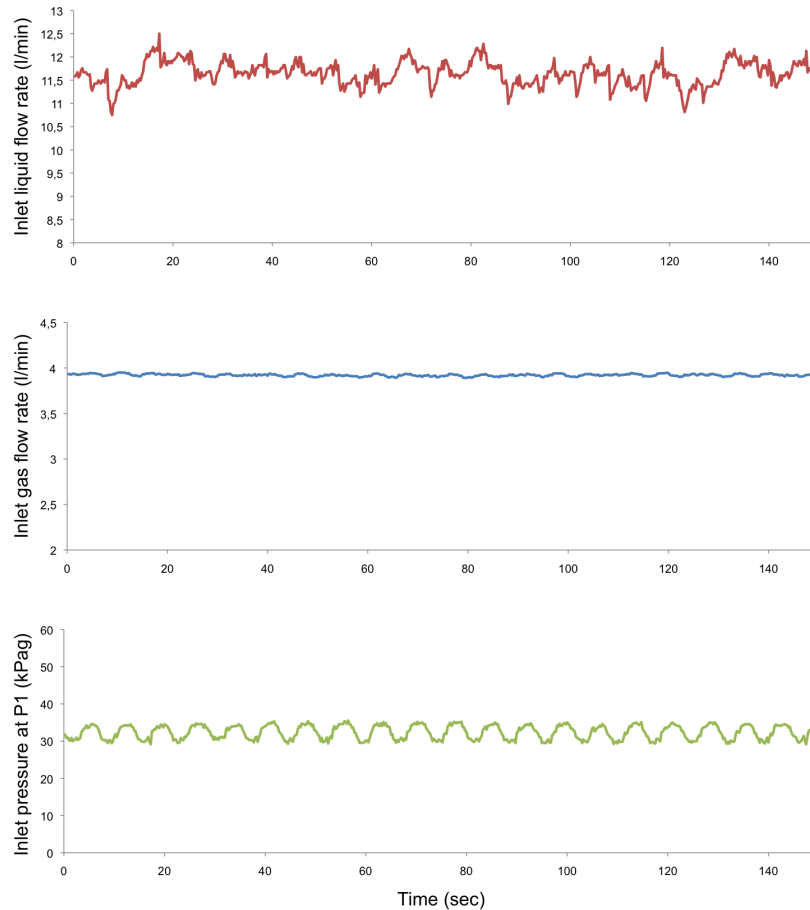


Figure 4.5: Logged data at liquid flow rate at 12 l/min and gas flow rate at 4 l/min, illustrating severe slugging type II flow regime.

Comparing figure 4.4 and 4.5, it is clear that the severe slugging II region had a higher frequency of slugging. In figure 4.5c the pressure build up was smaller and the slugging more frequent.

The type II slugging was less severe than the type I even though the inlet liquid flow rate had large variations. Receiving facilities are often constructed to handle the type II slugging regime.

When decreasing the gas flow rate in the severe slugging II region, the flow regime moved towards bubble flow. This flow type was continuous, and arose when the gas flow rate was small compared to the liquid flow rate. The gas formed small bubbles at the inlet that were continuously pushed through the system by the high liquid flow rate. Figure 4.6 illustrated this flow regime at liquid velocity of 12 l/min and gas velocity of 2 l/min.

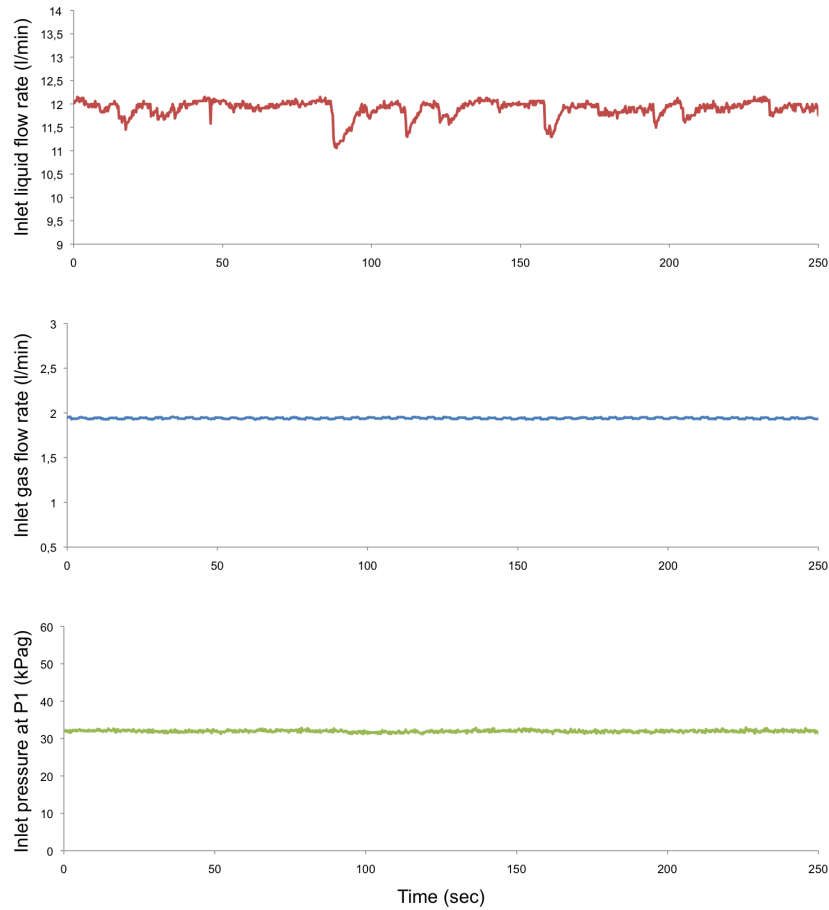


Figure 4.6: Logged data at liquid flow rate at 12 l/min and gas flow rate at 2 l/min, illustrating bubble flow.

### 4.2.2 The severe slugging type I cycle

Figure 4.7 illustrates the pressure at the inlet and in the buffer tank, and the volumetric flow rate of air and water. These plots are from the modified experimental setup. This figure is included to discuss how these parameters vary with the slugging cycle. The slugging cycle can be viewed in figure 2.1, section 2.1.

The slug was initiated by liquid accumulation at the low point of the riser, blocking the gas flow. At this point the inlet pressure immediately started to build up as no gas escaped through the riser. The pressure at the inlet built up faster than the pressure in the buffer tank because the pipe connecting the buffer and inlet had a small diameter (0.004 m) compared to the rest of the system (0.02 m). This caused the liquid to rise up to a certain height in the connecting pipe (see figure 4.8), to balance the following equation:

$$p_1 = p_3 + \rho_w g h_1' \quad (4.1)$$

As the liquid slug was growing, the pressure in the buffer tank increased, pushing the liquid column in the gas inlet pipe downwards. At the same time as the liquid column in the riser was growing, the liquid volume in the inclined section increased, causing the difference in the inlet pressure to be small. This is illustrated in figure 4.8, where the slug increased from  $h_1$  to  $h_2$  in the riser.

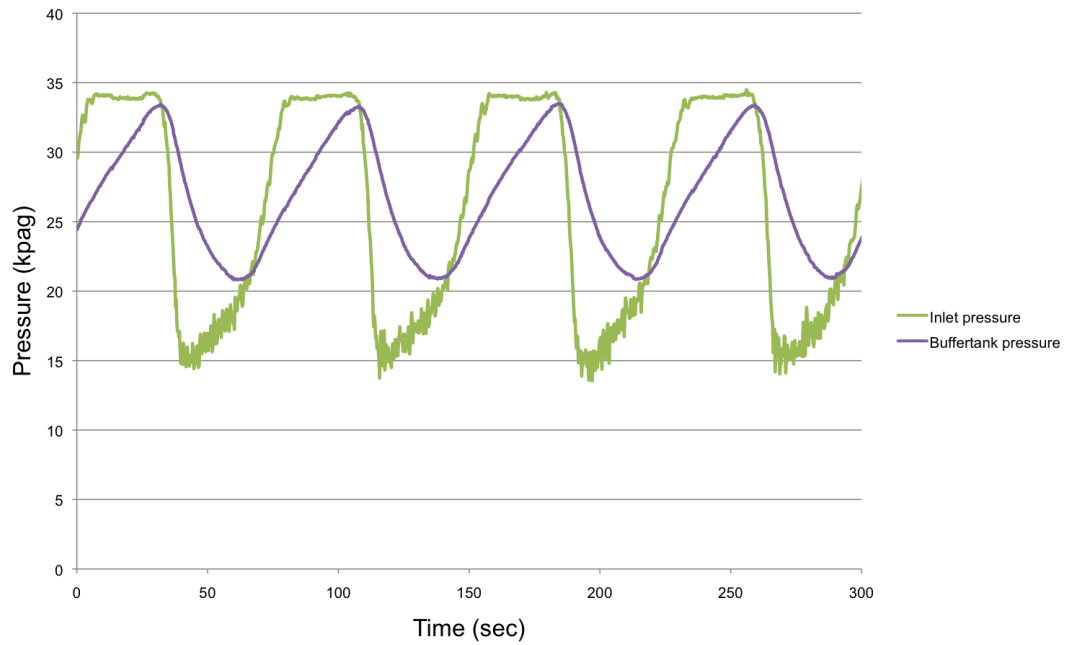
When the pressure build up in the buffer tank was high enough, the gas flow blew the liquid slug out of the riser. At this point the inlet pressure decreased rapidly, while the pressure in the buffer tank decreased at a lower rate. This was because the tube between the buffer tank and the mixing point had a much smaller diameter compared the the rest of the system. A smaller pipe diameter gives higher gas flow velocities and a higher frictional pressure drop. If the connecting pipe had a large diameter, the pressure in the buffer tanks would be equal to the inlet pressure. To find the pressure drop due to friction losses, equation 4.2 was used [15]. Equation 4.2 is derived in appendix C.

$$\Delta p = \lambda \cdot \rho \cdot \frac{v^2}{2} \cdot \frac{L}{D} \quad (4.2)$$

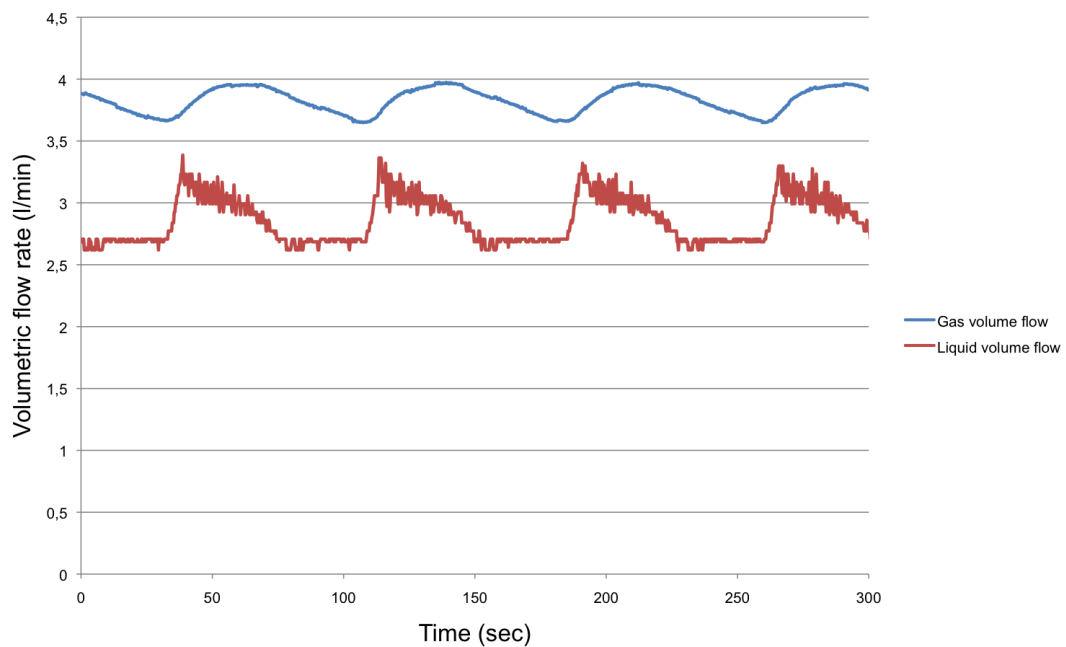
where:

- $\Delta p$  is the frictional pressure loss (Pa)
- $\lambda = 0.3 N_{Re}^{-0.25}$
- $N_{Re} = \frac{\rho v L}{\mu}$
- $\rho$  is the density ( $\text{kg/m}^3$ )
- $v$  is the velocity of the flow (m/s)
- $L$  is the length of the pipe (m)
- $\mu$  is the dynamic viscosity ( $\text{kg/m s}$ )
- $D$  the diameter of the pipe (m)

At a volumetric gas flow rate of 4 l/min and a diameter of 0.004 m, the velocity of the air was 6.7 m/s in the connecting pipe. This gives a pressure drop of 0.312 kPa. The calculation is illustrated in appendix C. Even though the frictional pressure drop was smaller than the pressure difference in figure 4.7a, it is reasonable that it takes longer time for the pressure to drop in the buffer tank compared to the inlet point that is directly connected to the riser.



(a) Pressure in buffer tank and at the inlet.



(b) Inlet gas and liquid flow rate.

Figure 4.7: Plots from experiment with gas flow rate at 3 l/min and liquid flow rate at 4 l/min.

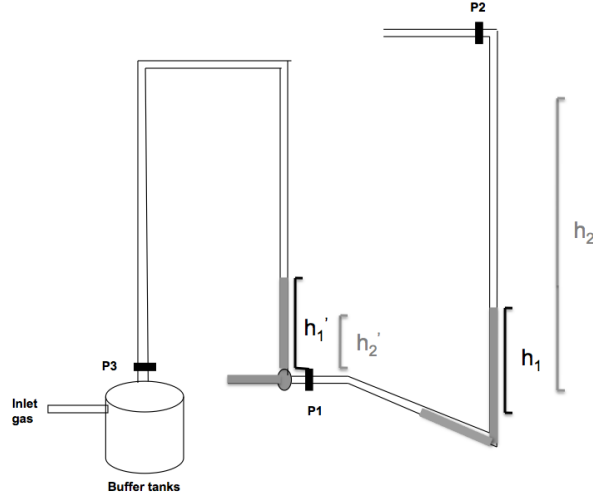


Figure 4.8: Illustration of liquid levels during slugging.

Comparing figure 4.7a and 4.7b, it is clear the the liquid flow reached a maximum during the blowout of the liquid slug. The volumetric gas flow was highest when the pressure was at the low point because of expansion. The flow meter for air was located upstream the buffer tank, so the gas flow rate was highest when the pressure in the buffer tank reached a minimum.

The fallback time is the time it takes for the inlet pressure to increase from the minimum point to the maximum pressure where it stabilizes. In this period of time, a liquid film is passing down through the riser. This phenomenon occurred after the main slug had been blown out of the riser (step 4 in the slugging cycle). Table 4.1 gives the fall back time ( $T_1$ ) and the full slugging period ( $T$ ) for different flow rates of water and air in the slugging type I region.

Table 4.1: Fallback time and slugging period for different flow rates.

$Q_L$ (l/min)	$Q_G$ (l/min)	$T_1$ (sec)	$T$ (sec)
2	5	55	91
2	4	47	100
2	3	42	133
2	2	39	163
3	4	40	77
3	3	34	90
3	2	30	136
4	4	27	55
4	3	23	67
4	2	25	115

As mentioned earlier, the period for the slugging cycle increased as the gas flow rate decreased. This is because it took a longer time to build up the required pressure for a blow out when the gas flow rate was low. The fall back time decreased when the gas flow rate was lowered. The fallback period is the time from the liquid slug is blown out of the riser to a new blockage at the low point is formed. As the gas flow rate decreased the gas' ability to push through the blockage decreased, and the time to form a new blockage was shorter.

### 4.2.3 Flow regime map

As mentioned, the pressure in the riser varied with the liquid and gas flow rate. This affects the flow rate of the gas. When constructing the flow map, the parameters are given in standard conditions. The ideal gas law (equation 4.3) was used to recalculate the gas volume flow to atmospheric pressure and standard temperature.

$$pV = nRT \quad (4.3)$$

The variables and parameters in this equation are:

p - pressure

V - volume

n - mole

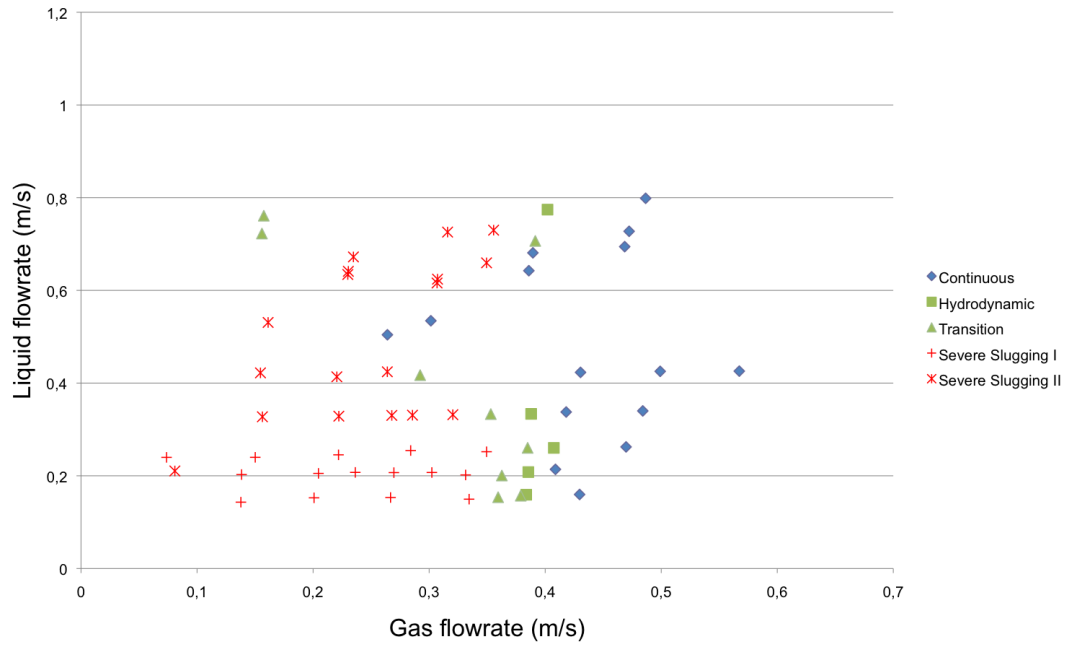
R - const

T - temperature

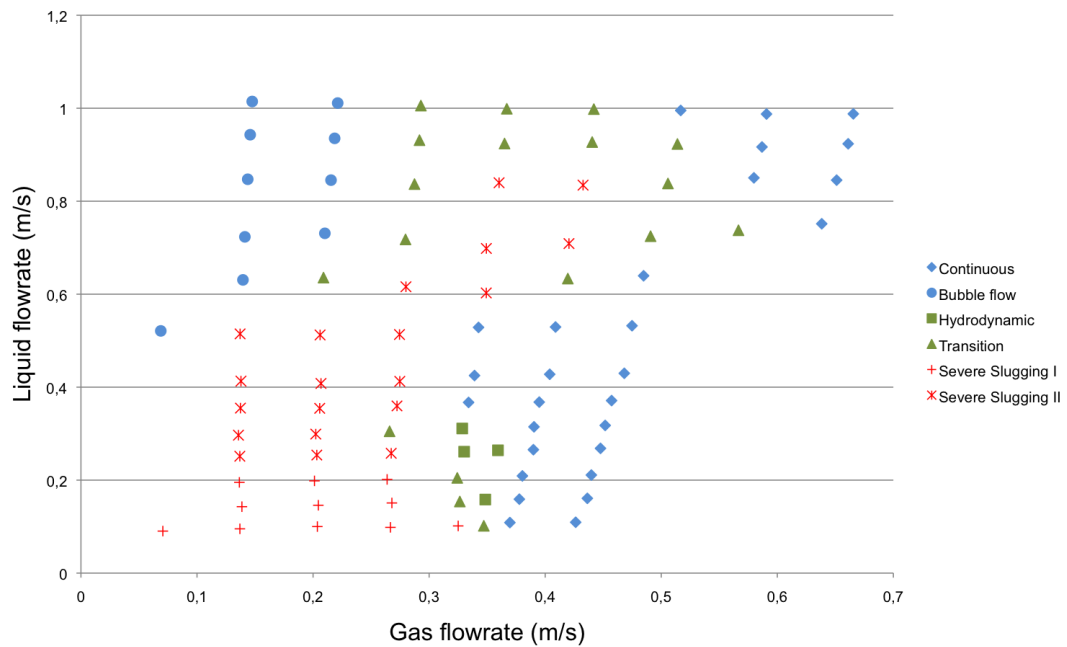
All the constant variables were moved over to the right hand side, giving equation 4.4 used to transform the volume flow of gas into standard conditions:

$$\frac{p_{ex}V_{ex}}{T_{ex}} = \frac{p_0V_0}{T_0} = constant \quad (4.4)$$

After the gas volume flow had been calculated into standard conditions, both the liquid and gas flows were converted into velocity unit (m/s). An example of this calculation is given in appendix D.1. The results from the flow-regime map experiments with both the original and modified setup will be discussed. Figure 4.9a illustrates the flow map from the original setup. After modifying the experimental setup, the flow map changed. The result of the modified setup is given in figure 4.9b.



(a) Flow-regime map from original setup.



(b) Flow-regime map from modified setup.

Figure 4.9: Flow regime map from the open-loop experiments.

The three colors represents different states of the flow. Blue is the continuous stable flow, green is a transition state and the red color indicates unstable slug flow. In the modified setup, bubble flow was observed at high liquid velocities and low gas flow rates. This flow is continuous, and is marked by blue circles. The transition state is divided into hydrodynamic slugging and a transition between two flow regimes. In figure 4.9 the unstable region is divided into severe slugging type I and II. The type I slugging is marked by crosses and type II by stars.

The flow regime moves from a continuous flow towards the severe slugging region when decreasing the gas flow. If the gas flow is decreased beyond the slugging region, the flow regime would move towards a continuous flow as the gas flow approaches zero. This is not feasible to test on the miniloop riser. However, this trend can be observed in the severe slugging type II region. Decreasing the gas flow rate beyond this region, bubble flow occurred. In the flow regime map, the severe slugging type II region can be found at a liquid flow from 0.26 m/s and up in the modified setup, and from 0.33 m/s in the original.

In the original setup, the main concern was that liquid was flowing into the buffer tanks. As illustrated in section 3.1, this problem led to inconsistencies in the results. It was possible to extend the experiment to higher liquid velocities because no water was flowing into the buffer tanks after the modifications, this created a clear boundary for the severe slugging type II region. In figure 4.9b, the severe slugging type II does not exist when the liquid flow rate increased to a sufficiently high velocity. The transition state at these high water flow velocities was a transition between continuous and bubble flow.

As mentioned earlier, the flow regime depends on the geometry of the riser in addition to the liquid and gas flow rate. Comparing the flow regime map in this thesis (figure 4.9b) to earlier research from Taitel et. al. [12], the similarity is that severe slugging type I exists at low liquid and gas flow rates. The boundaries are shifted because of different geometries and conditions.

#### 4.2.4 Analysis of experimental data

When the flow regime was in the severe slugging region, there was a pressure build up in the buffer tank for each cycle. In the modified loop, the pressure sensor P3 was placed between the two buffer tanks. In figure 4.10, the maximum, minimum and differential pressure is plotted for a constant gas flow rate of 3, 4 and 5 l/min. The liquid flow velocity is on the horizontal axis.

Looking at the maximum and minimum pressure in the buffer tank, it is clear the the amplitude of P3 decreased when the liquid flow velocity increased. This is because the flow regime moved from a severe slugging type I to type II at higher liquid flow rates.

Looking back at the different types of flow regimes in section 4.2.1, the differences between severe slugging type I and type II were presented. In the severe slugging type II region, the gas flow rate variations decreased while the liquid flow became more unstable. The time period between each slug decreased, causing the pressure build up in the buffer tanks to decrease as well. This is reflected in figure 4.10, at a liquid flow rate of 0.26 m/s the pressure amplitude in the buffer tanks was small.

When comparing figure 4.10 to the flow regime map (figure 4.9b), the x-axis in figure 4.10 is the

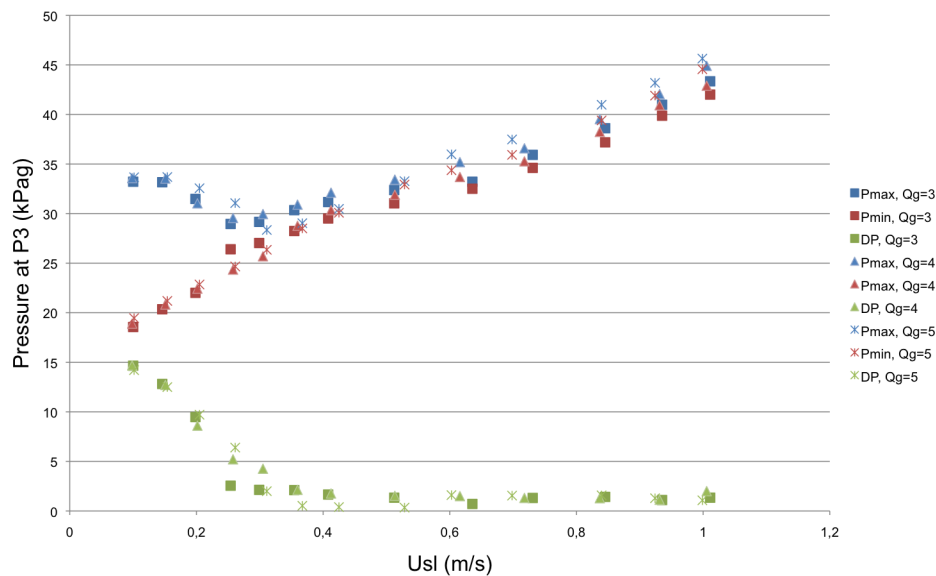


Figure 4.10: Amplitude plot at P3 with constant gas flow rate of 3, 4 and 5 l/min.

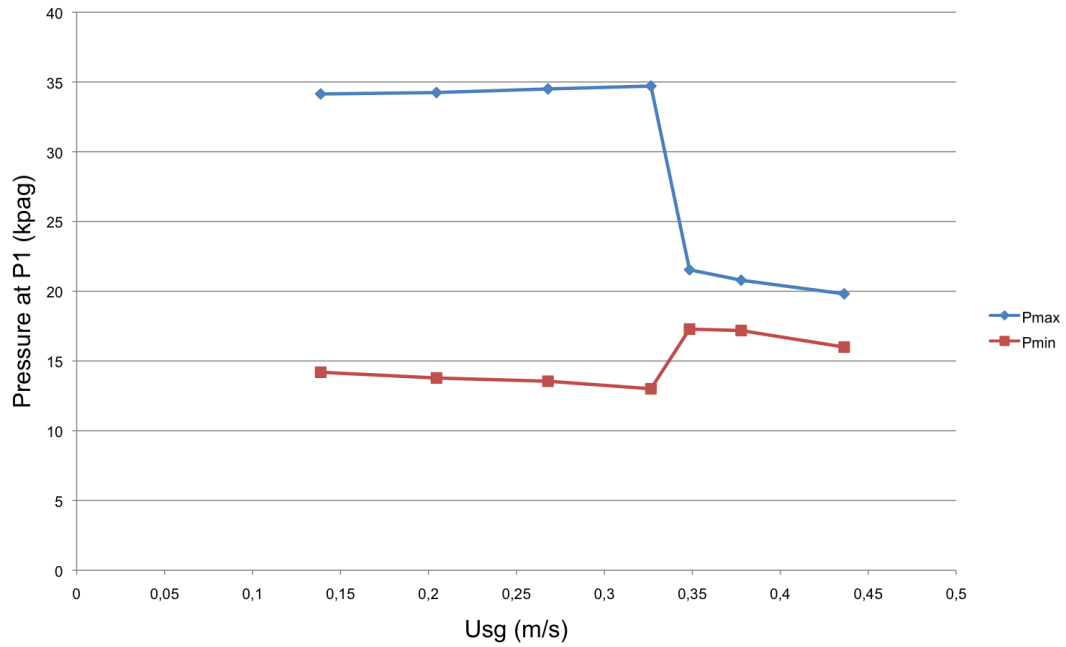
y-axis in figure 4.9b. In the flow regime map, the severe slugging type II region existed at liquid flow rates of 0.26 m/s and above. At this point, the differential pressure in the buffer tanks had decreased to 5 kPa (0.05 bar).

In figure 4.10 the gas flow rate was held constant at three different values. It is also interesting to study how the inlet pressure and the time-period between slugs vary with the gas flow rate when keeping the liquid flow constant. In figure 4.11a and 4.11b the water flow rate is held constant at 3 l/min (0.16 m/s).

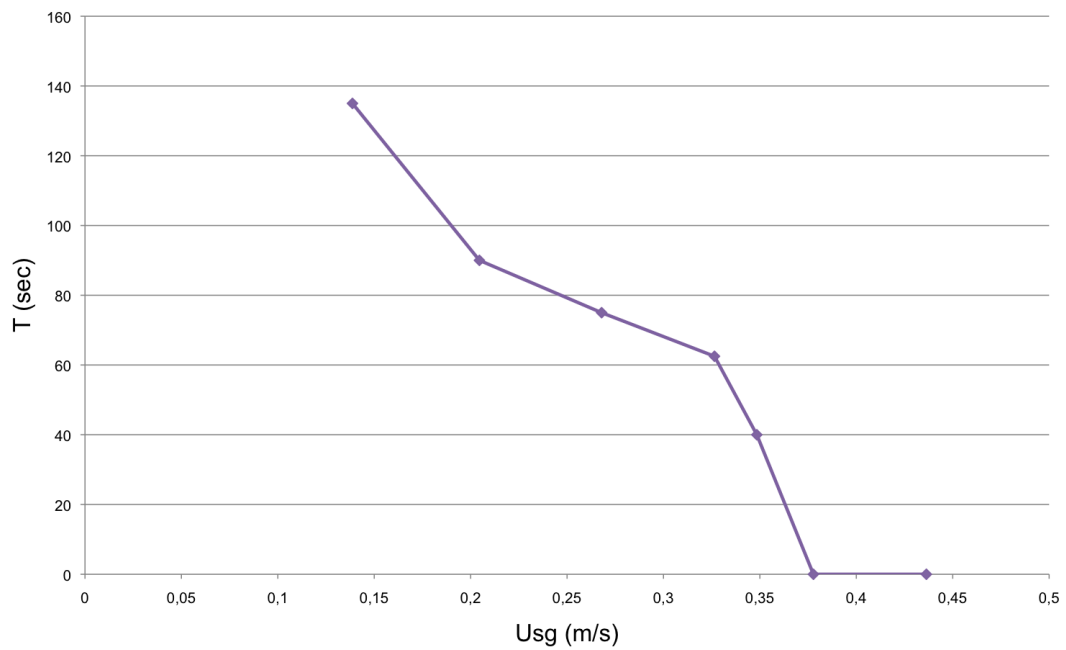
In the amplitude plot (figure 4.11a), the maximum and minimum inlet pressure is plotted with varying gas flow rate. There is a clear jump in the amplitude from 0.32 to 0.35 m/s. The flow regimes at these two points were transition state and hydrodynamic slugging, respectively. In the hydrodynamic slugging regime, the liquid and gas flow rate were close to constant and the pressure was oscillating with a small amplitude. Moving in to the transition state, every other oscillation was a hydrodynamic and a severe slug. It is the maximum amplitude, meaning the amplitude from the severe slugs, that is plotted in figure 4.11a.

Figure 4.11b illustrates how the time-period in the slugging oscillations varied with the liquid flow velocity. The flow regime moved from a continuous flow regime to severe slugging when decreasing the water flow. The two last points in the plot are zero because the flow was continuous with no oscillation. The hydrodynamic slugging is not as easy to spot in the period plot as in the amplitude plot.

Comparing the two figures at constant liquid flow rate (figures 4.11b and 4.11a), the amplitude in the severe slugging region did not vary much with the gas velocity in severe slugging type I, while the time-period did. This means the difference between the slugging behavior at each gas velocity was the time it took to build up a high enough pressure to blow out the liquid column in the riser. The magnitude of the pressure amplitude did not change when the liquid flow rate was constant. When the flow rate of the water changed, the pressure amplitude changed.



(a) Amplitude plot with constant liquid flow.



(b) Period plot with constant liquid flow.

Figure 4.11: Amplitude and period plot for a constant liquid flow rate of 3 l/min.

### 4.3 Sources of error

When conducting experiments, experimental errors can arise in the form of inaccurate values. The accuracy of the values in this experiment depend on the calibration of equipment. If it is assumed the accuracy of time-taking was 1 second, the accuracy for 1 l/min would approximately be  $\pm 0.02$  l/min. This calculation is given in appendix E.1. Transforming the errors to the liquid velocity (m/s), all the errors were in the magnitude  $10^{-3}$  m/s. Deviations of this size will not effect the points in the flow regime map considerably. The pressure calibrations are assumed to be highly accurate. The results during this calibration were produced from the calibration device and the logged data in LabVIEW.

The variations in the liquid flow rate at a continuous flow increased with higher flow rates. Appendix E.2 lists the average flow rates with the corresponding deviations at a gas flow rate of 7 l/min to keep all the points in the continuous region. It is clear that by increasing the flow rate of water from 14 l/min to 16 l/min, the deviations increase considerably from  $\pm 8$  % to  $\pm 15$  %. This phenomenon was caused by inaccuracies from the flow meter measurements when the flow rate approached the upper limit of the measurement device of 20 l/min. Increasing the liquid flow rate also increased the turbulence of the flow in the pipe.



# Chapter 5

## Closed-loop experiment

This section describes the experiments with the top valve (CV in figure 3.1) used for closed-loop pressure control. The flowsheet for the control scheme is illustrated in figure 2.2, section 2.2. The closed-loop flow regime map from both the original and modified miniloop will be presented, while all other results are from the modified setup.

### 5.1 Experimental

#### 5.1.1 Closed-loop flow regime map

After the open-loop flow regime map was identified, a feedback controller was added to the system to find the points within the severe slugging region that could be controlled. First the experiments were conducted with a P-controller, and then a PD-controller with filter. The inlet pressure was the controlled variable and the valve opening the manipulated variable.

#### 5.1.2 Bifurcation map

When conducting the bifurcation map experiment, both the liquid and gas flow rates remained constant. In this experiment the liquid and gas flow rates were set to 4 l/min. At this point the flow regime was severe slugging type I when the valve was completely open.

First the pressure versus valve opening was logged with manual control, by adjusting the valve opening. The pressure measurement used in this experiment was the inlet pressure (P1 in figure 3.1). In this part of the experiment, the valve opening was decreased from 100% to 6% opening. The pressure was not adjusted, but varied with the valve opening.

Next a PI-controller was added to the system. The set point of inlet pressure P1 was the degree of freedom. The "stable" region with the controller was found by decreasing the set point until the flow regime entered the "unstable" region. The starting point of the set point was 35 kPag.

## 5.2 Results and discussion

All the logged data during this experiment is enclosed in appendix A.

### 5.2.1 Set point adjustment with P-control

The P-controller proved to be most stable during the closed-loop experiments. The parameters in this controller were the inlet pressure set point value and the gain. Because the goal of this experiment was to stabilize the flow regime, the controlled variable offset was not an issue as long as the pressure stabilized.

As mentioned earlier, the severe slugging is reduced by choking the top side valve and increasing the upstream pressure. Figure 5.1 illustrates how increasing the set point value stabilized the pressure. This plot is from the modified setup.

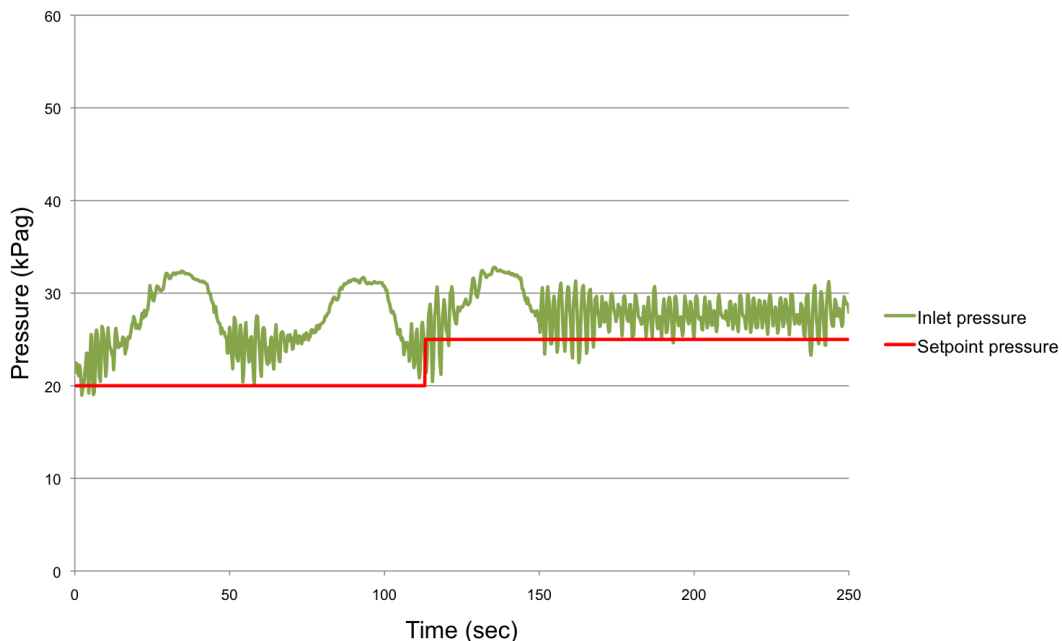


Figure 5.1: Illustration of how the set point effects the stability at liquid flow rate of 4 l/min and gas flow rate 3 l/min.

When the set point pressure was 20 kPag the controller tried to keep the inlet pressure constant at a value where slugging would occur. When increasing the set point, the average valve opening decreased. At this point the inlet pressure was raised to a value where the gas flow was able to penetrate the liquid in the riser.

The pressure at which the flow regime stabilized increased as the gas flow rate decreased and the period between each slug increased. Increasing the liquid flow rate also increased the stabilized inlet pressure.

### 5.2.2 Filtering P1 measurements

In the beginning of the experiments, a P-controller was implemented to test what severe slugging points were controllable. The next step was to test the uncontrollable points with a PD-controller. Before this could be done, it was necessary to add a filter to the inlet pressure measurements to remove noise. This is explained in section 2.2. Figure 5.2 illustrates the effect of the filter.

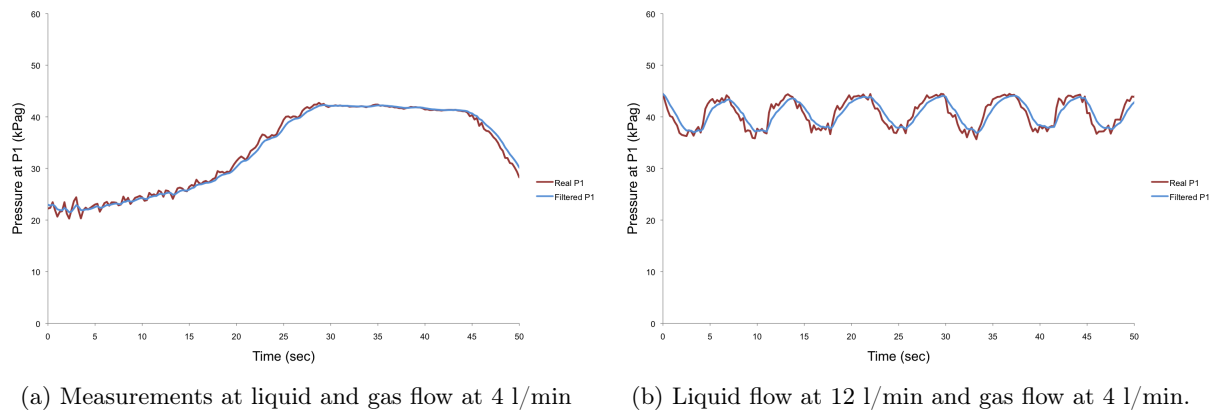


Figure 5.2: Comparison of real P1 and filtered P1 measurements.

The red line is the unfiltered and the blue line the filtered measurement. The filtered values of the P1 measurements had a smoother curve than the real values, and the time delay from the real measurements to the filtered values were small.

### 5.2.3 PD-control versus P-control

The implementation of the PD-controller did not seem to improve the qualities of the controller, and was not able to stabilize flow regimes that the P-controller failed to stabilize. This section is included to illustrate this result. Figure 5.3 and 5.4 compares the effect the two controllers had on the severe slugging flow, type I and type II. The controlled variable (P1) and the valve opening is plotted for both cases, the P-control to the left and PD-control to the right.

Figure 5.3 illustrates the controllers action on the severe slugging type I flow regime. It is clear that the P-control was most effective in this case. The PD-controller was able to eliminate the severe slugging flow, but not the oscillations in the pressure at P1. Another negative effect of the PD-controller was large variations in the valve opening. It continuously jumped between fully closed and an opening of 50-60%. This would wear and tear on the choke-valve and eventually result in equipment failure.

The severe slugging type II flow proved to be hard to control because of the high frequency. Figure 5.4 illustrates the effect of the two controllers on this flow regime.

The P-controller was able to decrease the pressure variations at the inlet, but with large variations in the valve-opening. Comparing the performance with the PD-controller, both the pressure-

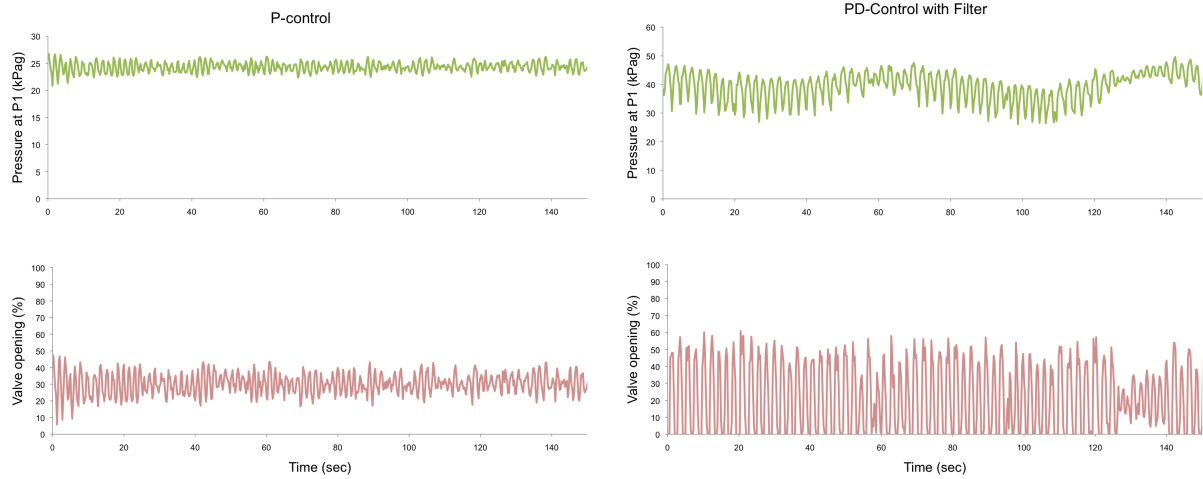


Figure 5.3: A comparison of P-control (to the left) and PD-control (to the right) at liquid velocity of 4 l/min and gas flow of 4 l/min.

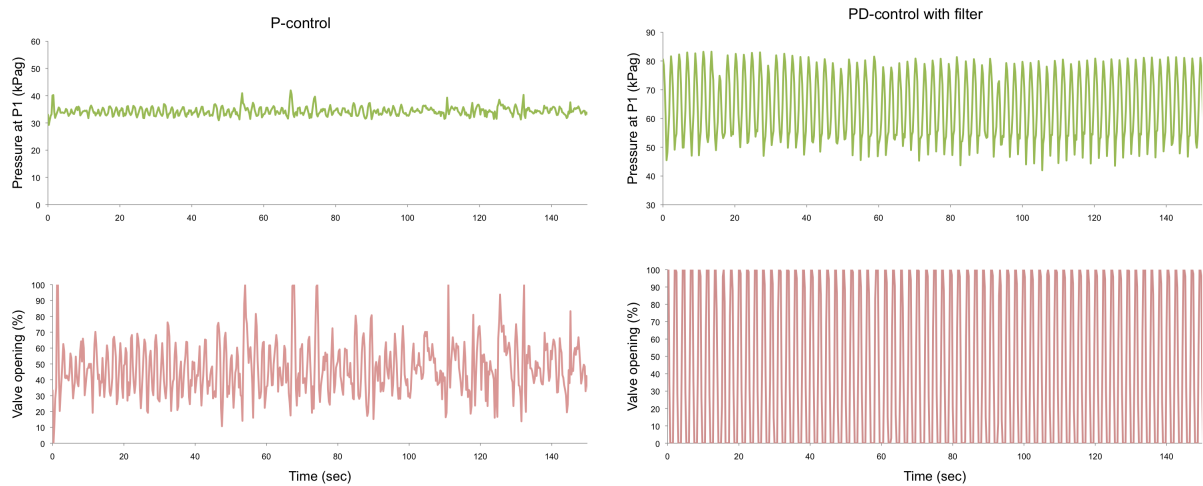


Figure 5.4: A comparison of P-control (to the left) and PD-control (to the right) at liquid velocity of 12 l/min and gas flow of 4 l/min.

and valve opening variations increased with the PD-controller. It is not desirable that the valve opening jumps from fully open to fully closed over a longer time period.

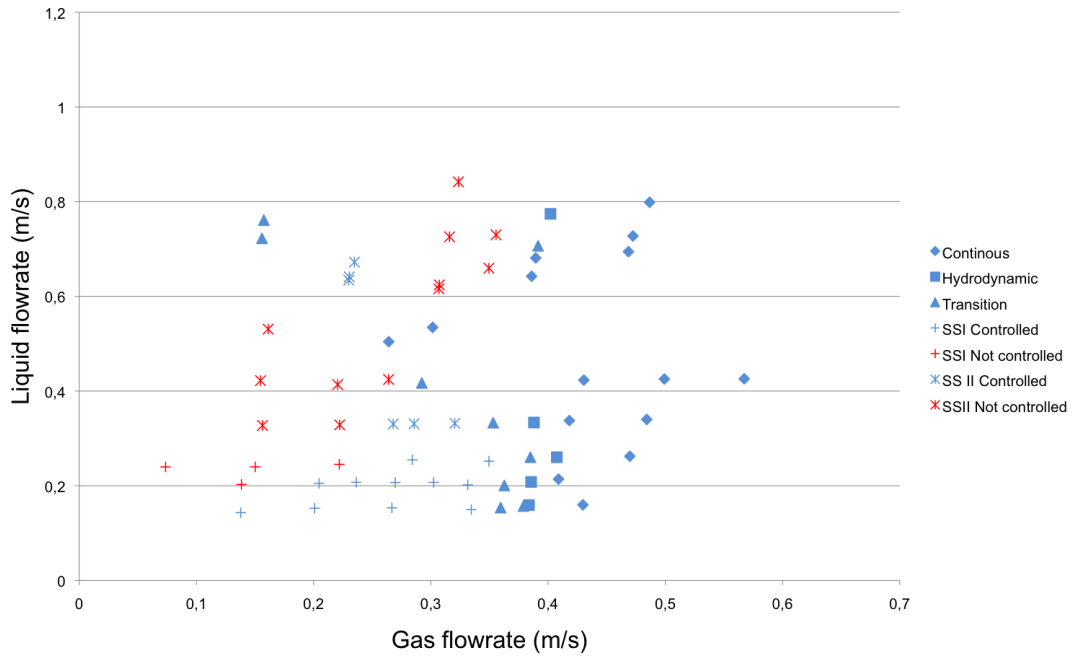
It is important to keep in mind that the PD-controller was harder to tune manually because of the extra controller parameter. The controller parameters used in the experiments illustrated in figure 5.3 and 5.4 are most likely not the optimal combination. However it was the most stable results that were obtained during these experiments.

#### 5.2.4 Flow regime map with controller

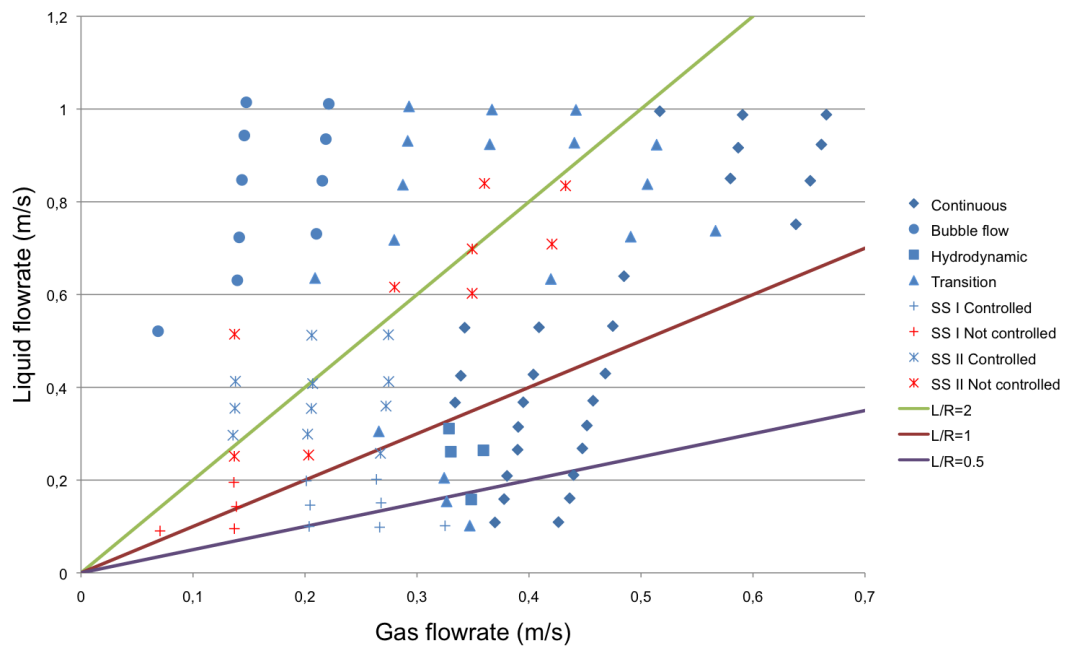
The steps for calculating the points in the closed-loop flow-map experiments were the same as described in the open-loop section. The results from the original and modified setup is illustrated in figure 5.5.

The blue points in the plot were the stable flow regime and points in the severe slugging region that were controllable. The red points were not stabilized with the controller. The three lines in the flow map for the modified setup are different liquid-to-gas ratios (L/R-ratios).

The values in this flow map can not be used for differently scaled systems, but give an indication of the flow behavior in the two-phase flows in risers.



(a) Flow-regime map from original setup.



(b) Flow-regime map from modified setup.

Figure 5.5: Results from the closed-loop experiments.

The purpose of this experiment was to see how far into the "unstable" region the operating conditions could be extended. On oil platforms, the system is designed to stay outside severe slugging flow regimes when no control is applied. Adding the control structure to the process, increases the operating areas in the flow regime map. By assuming that the L/R-ratio remains constant throughout the production period of the reservoir, it is possible to see how far the controller could extend the reservoir life. At a L/R-ratio of two, the flow regime would move through the severe slugging II region. If the receiving facility is constructed to handle this type of flow, the production could be extended to a liquid flow velocity of 0.25 m/s and a gas flow velocity of 0.13 m/s. This is the boundary to the severe slugging type I region, meaning the controller would not effect the operating area for this liquid-to-gas ratio. Looking at the L/R-ratio of one, the flow regime would move into the hydrodynamic and transition state at a liquid flow velocity of 0.31 m/s and gas flow velocity of 0.32 m/s. In open-loop operation, this point would be the boundary of where the production would have to stop. By adding the controller, the production could continue until the velocity of liquid was 0.14 m/s and 0.13 m/s for the gas flow. At a L/R-ratio of 0.5 the operating area was extended from a liquid flow velocity of 0.15 m/s and a gas flow velocity of 0.32 m/s to 0.1 m/s for the liquid flow and 0.13 m/s for the gas flow velocity. These values are summarized in table 5.1. Because of the limitations in the measurement equipment in the experimental setup, values below 0.09 m/s could not be measured for the liquid flow. Keep in mind that the profit of producing at low liquid and gas flow rates compared to the cost of running a receiving or production unit is not considered in this thesis.

Table 5.1: Boundary to severe slugging type I for open-loop and closed-loop operation.

L/R-ratio	Open-loop		Closed-Loop	
	U <sub>sg</sub> (m/s)	U <sub>sl</sub> (m/s)	U <sub>sg</sub> (m/s)	U <sub>sl</sub> (m/s)
2	0.25	0.13	0.25	0.13
1	0.31	0.31	0.13	0.14
0.5	0.31	0.15	0.13	0.1

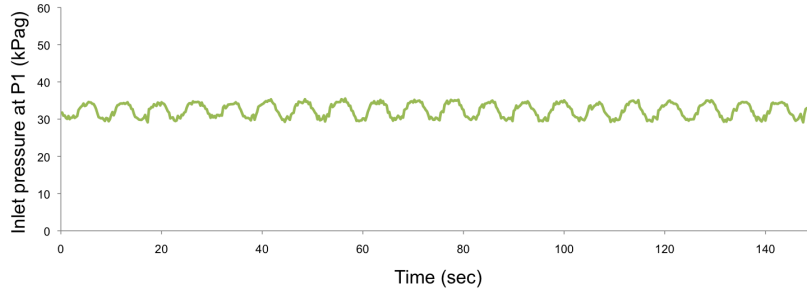
Comparing the two closed-loop experiments, the similarity is that the flow regime became hard to control at low gas flow velocities and in severe slugging type II region. In the severe slugging type II region, the liquid fluctuations were high and rapid. The pressure amplitude was smaller than in the severe slugging type I region, but the time periods were shorter and the pressure was at a higher level. This is illustrated in table 5.2, where the frequency and amplitude are compared for slugging at a liquid flow of 3 l/min (0.15 m/s) and 12 l/min (0.63 m/s), representing severe slugging type I and II respectively.

Table 5.2: Comparison of frequency and inlet pressure amplitude for severe slugging type I and II.

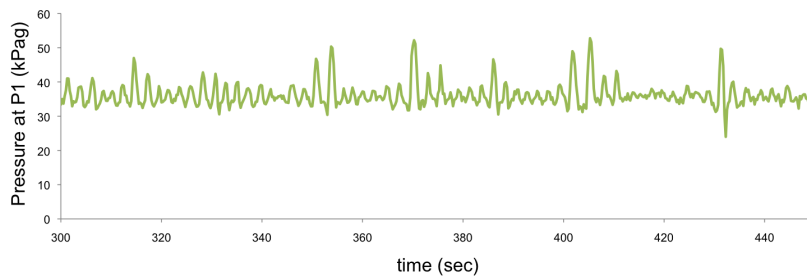
Slugging Type	I	II
Frequency (s <sup>-1</sup> )	0.07	0.9
$\Delta p$ (kPag)	20.5	6.8

When the frequency became too high, the system was hard to control. This explains the control difficulties in the severe slugging II region. Adding the controller to the severe slugging I region at very low gas flow rates, the control valve almost closed completely in order to increase the pressure at the inlet.

When adding a controller to the system in the severe slugging II region, the maximum amplitude of P1 increased and the fluctuations became more rapid and irregular. This is illustrated in figure 5.6. The plot of the pressure at P1 without control is the top figure, and with P-control in the bottom.



(a) Pressure measurements with no controller.



(b) Pressure measurements with controller.

Figure 5.6: The effect of control on the severe slugging II region at liquid flow rate of 12 l/min and gas flow of 4 l/min.

The pressure in figure 5.6b was not stabilized by the controller.

### 5.2.5 The gain of the controller

The dynamic controller stabilized the flow regime by adjusting the top side valve opening. Compared to manually choking the valve to eliminate severe slugging, the dynamic controller minimized the pressure drop over the valve and increased the production rate. The pressure in the pipe upstream the riser is called back pressure. This pressure is equal to the inlet pressure for this experimental setup. Decreasing the back pressure during control, increases the production rate by opening the choke valve and minimizing the liquid holdup in the riser.

Table 5.3 gives the maximum pressure in the open-loop ( $P_{max,OL}$ ) and closed-loop setup ( $P_{max,CL}$ ) and the difference in percentage (DIFF) for various flow rates of water and air. The slugging period (T) and the flow regime are also listed in the table. Only some of the points in the flow regime map that were controlled are listed in this table.

Table 5.3: Decrease in back pressure with closed-loop setup.

$Q_L$ (l/min)	$Q_G$ (l/min)	T (sec)	$P_{max,OL}$ (kPag)	$P_{max,CL}$ (kPag)	DIFF (%)	Regime
2	5	91	33	26	21.2	SS I
2	4	100	33	25.5	22.7	SS I
2	3	133	33	29	12.1	SS I
3	4	77	34.5	28	18.8	SS I
3	3	90	34	30.3	10.9	SS I
4	4	55	32	27	15.6	SS I
4	3	67	32	31	3.1	SS I
6	3	13	32	38	-15.2	SS II
6	2	16	32	38	-18.8	SS II
8	4	9	35	41	-17.1	SS II
8	3	11	35	41	-17.1	SS II
8	2	11	34	42	-23.5	SS II
10	4	8	32	42	-27.3	SS II
10	3	9	32	39	-21.9	SS II
10	2	10	31	35	-12.9	SS II

The back pressure decreased with approximately 10 to 20 percent with the dynamic controller, when the open-loop flow regime was severe slugging type I. Adding a controller to the severe slugging type II flow pattern increased the pressure upstream the riser. Even though the pressure increased after adding the controller, the magnitude of the flow rate oscillations decreased. Considering that type II slugging is less severe than the type I, the gain of adding the controller might not be valuable. A higher back pressure versus a more steady flow must be evaluated for the separate receiving facilities.

### 5.2.6 Bifurcation map

One purpose of this experiment was to investigate how the dynamic controller increased the production rate by increasing the choke valve opening while keeping the flow stable. The liquid and gas flow were fixed at 4 l/min. In the experiment with manual control, the valve-opening was the only degree of freedom. When adding the dynamic controller, the set point value for P1 became the degree of freedom. The average value for the valve-opening was used when plotting the results from the experiments with control. The results are illustrated in figure 5.7. The minimum valve opening in this experiment was 6 %. Closing the valve beyond this point was not feasible for the miniloop.

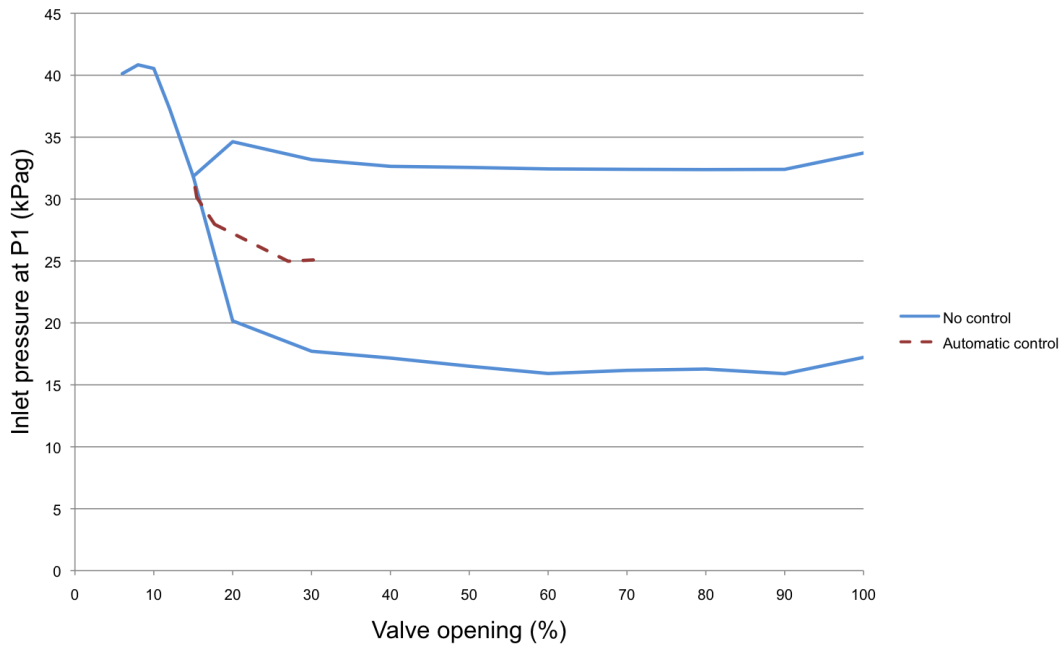


Figure 5.7: Result from bifurcation map experiment with liquid flow of 4 l/min and gas flow 4 l/min.

With manual control, the "stable" flow region existed up to a valve opening of 10 %. When opening the valve above this point without the dynamic controller, the flow regime went "unstable". Decreasing the valve opening increases the pressure drop over the choke-valve and limits the production because of a larger holdup upstream the choke-valve. When adding the dynamic controller, the stable region was extended to a valve opening of 30 %. Table 5.4 contains some results from the experiment, comparing values with a valve opening ( $Z$ ) at 10 % in manual mode and 30 % with control.

Table 5.4: Results from bifurcation experiment

Parameter	$Z=10\%$	$Z=30\%$ (with control)
Pressure at inlet (kPag)	40	25
Pressure at top of riser upstream valve (kPag)	18	4
Pressure drop over riser (kPa)	22	21
Pressure drop over valve (kPa)	18	4
Average inlet liquid flow (l/min)	3.2	3.8
Average inlet gas flow (l/min)	3.3	3.8

As mentioned earlier, the frequency and the amplitude determined if the system could be controlled. At the critical point of the valve opening the frequency was  $0.06 \text{ s}^{-1}$ . The pressure amplitude remained at a constant value of 16.5 kPag in the "unstable" region throughout the experiment. At a valve opening of 30 % the controller was no longer able to stabilize the flow regime. The frequency of P1 at a 30 % valve opening had increased to  $0.08 \text{ s}^{-1}$ .

### 5.3 Sources of error

The accuracy of the values in the closed-loop flow regime map are the same as in the open-loop experiment. This is discussed in section 4.3.

The major source of error in the closed-loop flow regime map is the uncertainty if the control parameters used were the optimal values. The controller was tuned by the "trial-and-error"-method, meaning that there most likely exist better control parameters for the points on the flow-map that were not stabilized.



## Chapter 6

# Comparison of experimental data with OLGA-model

OLGA is a dynamic simulator for oil-water-gas mixtures in pipelines. The program has a graphical editor, where models are constructed by the "Drag & Drop" method. The pipeline consists of nodes that can be connected by pathflows. Nodes can be inlets, outlets or mixing points. The positive direction of the flow must be defined. Equipment such as compressors, valves and pumps are available in the Process Equipment list.

When constructing a model, the flow path between nodes is divided into the desired amount of pipelines. The geometry of the flow path is defined by setting the starting and ending coordinates of each pipeline. These pipelines are divided into segments, which determines the accuracy of the calculations. OLGA calculates the outputs of each segment one at a time. Dividing the pipeline into smaller segments will give better results, but also increases the calculation time. [16]

When a case is run in OLGA, output files are produced. These outputs can be selected from a long list of variables.

### 6.1 The model

OLGA version 5.3.2.3 was used in this modeling work. The model built in OLGA was developed from a base case for severe slugging. The base case for severe slugging is described in appendix G. This model had the same geometry as the miniloop, except it did not include the buffer tank. Changes made to the base case were:

- Changing source from oil-gas mixture to water-air mixture. This was done by adding a PVT-tabular for a water-air mixture as an input. The PVT-table limited the conditions to 18 - 22°C and 100 - 5·10<sup>6</sup> Pa.
- Separating the water and air inlet into two different sources and adding a mixing point.

- Adding a buffer tank at the air inlet. The pipe connecting the buffer tank to the mixing point was modeled with the same elevation and diameter as in the miniloop.
- Adjusting parameters such as pipe lengths, temperature and pressure to fit the miniloop.
- Increasing the number of sections to get a higher accuracy of simulations.

A picture of the model in the graphical editor in OLGA is illustrated in figure 6.1. The four nodes in this picture are the inlet of water and air, mixing point and the outlet.

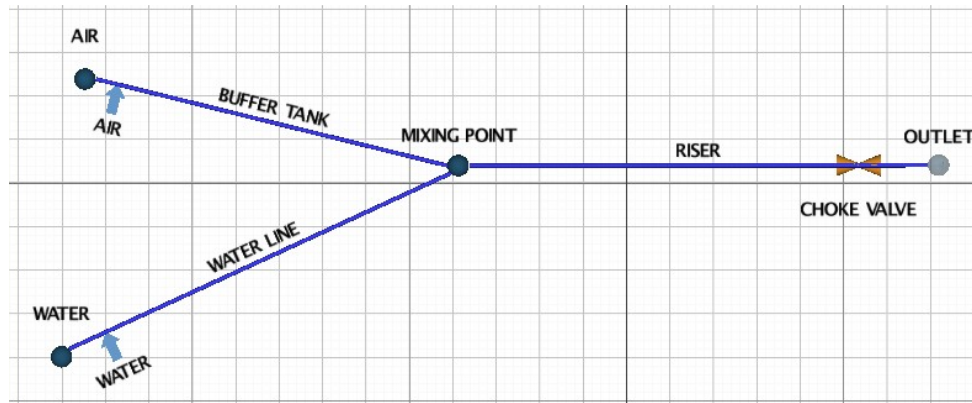


Figure 6.1: Snapshot of the model of miniloop in OLGA.

The inputs to the model were the flow rates of water and air, the ambient temperature (20 °C), the pressure at the outlet (1 bar) and valve opening for the choke-valve (100 % open). The flow rates of water and air had the unit kilograms per second (kg/s) in OLGA. When constructing the flow regime map in section 4.2.3, the flow rates were calculated from liters per minute (l/min) to meters per second (m/s) via cubic meters per second ( $\text{m}^3/\text{s}$ ). The last of these values ( $\text{m}^3/\text{s}$ ) was used to find the flow rate in kilograms per second.

## 6.2 Results

All the raw data from the simulations is enclosed in appendix A. The main trend of the results from the OLGA simulations compared to the experimental results was that the inlet pressures from the experimental results were higher than the simulated values, but the amplitudes were smaller. Figure 6.2 compares the inlet pressure at P1 in the severe slugging type I region. The flow rates of water and air are both 3 l/min (liquid velocity 0.15 m/s and gas velocity 0.2 m/s).

The red plot is the result from the simulations, while the blue plot is the inlet pressure from the experiment. As mentioned above, the experimental pressure was higher than the values from OLGA, but the difference in the maximum pressure was only 2 kPa. The pressure build up in buffer tank is dependent on the amount of liquid in the riser slug. Small inaccuracies in the riser height and the flow rates would have an effect on the simulation results.

Another difference is the period between each slug. In the simulation the period was 82 second, while in the experimental results it was 90 seconds. It is the volume of the buffer tank and the

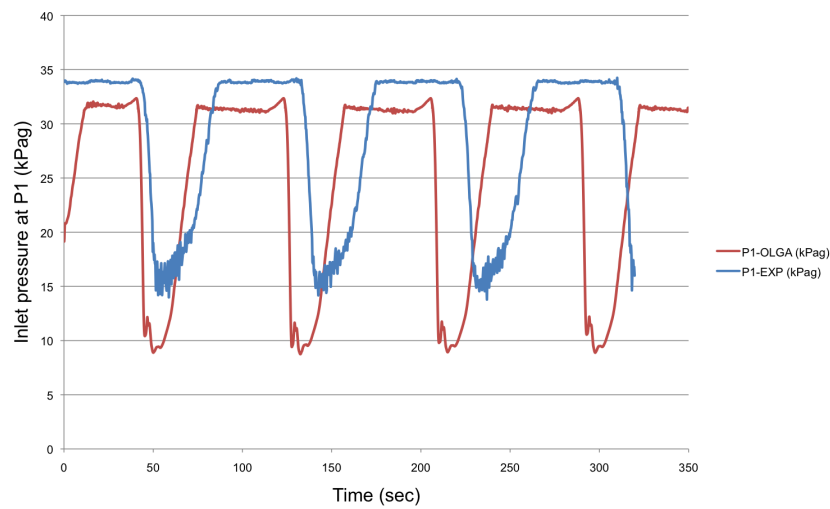


Figure 6.2: Comparison of simulation and experimental results of severe slugging type I at flow rates of gas and liquid at 3 l/min.

gas flow rate that effects the period the most. When building a model of the buffer tank in OLGA, the volume of the two tanks in the experimental setup were summed up to one large buffer tank. It is possible that the volume in the buffer tank was not the exact same as in the experiment due to inaccuracy in measurements and rounding errors.

Figure 6.3 compares the inlet pressure in the severe slugging type II region. The experimental results are plotted in blue.

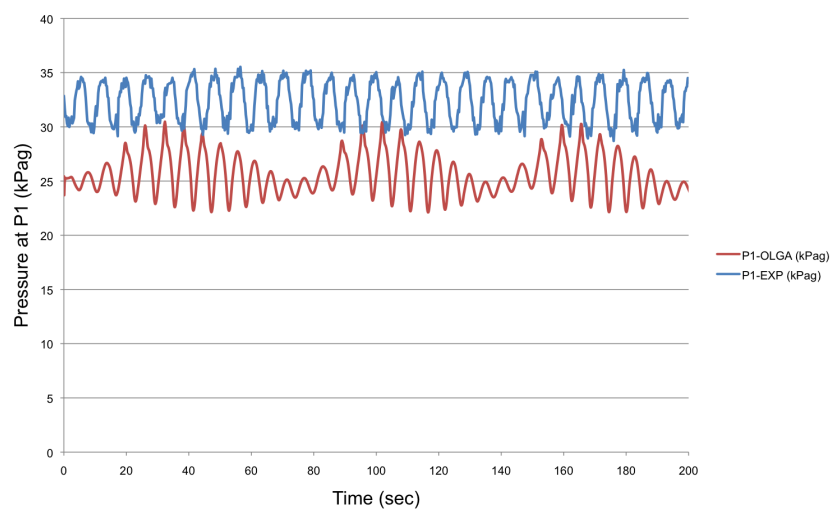


Figure 6.3: Comparison of simulation and experimental results of severe slugging type II, for liquid flow rate at 12 l/min and gas flow rate of 4 l/min.

In figure 6.3 the amplitude in the experimental result was 7 kPa, while the simulations gave an amplitude of 8.4 kPa. This figure clearly illustrates the difference in the average pressure. The average pressure was 32 kPag for the experiment and 26 kPag for the simulation. The main

difference at this point in the flow regime map was that the inlet pressure in the simulation was oscillating between smaller and larger amplitudes. At these conditions, the simulator was showing a flow regime similar to the pseudo-steady regime "cyclic oscillation with fallback" defined by Taitel et al. [13](see section 2.1). Increasing the liquid flow from this point in OLGA, the pressure showed the same behavior as the experimental results.

Increasing the liquid flow above the severe slugging type II region, the flow regime stabilized. Figure 6.4 illustrates the inlet pressure when the liquid flow is 20 l/min (1 m/s) and the gas flow is 5 l/min (0.4 m/s). This point can be found at the top of the flow regime map, in the continuous flow region.

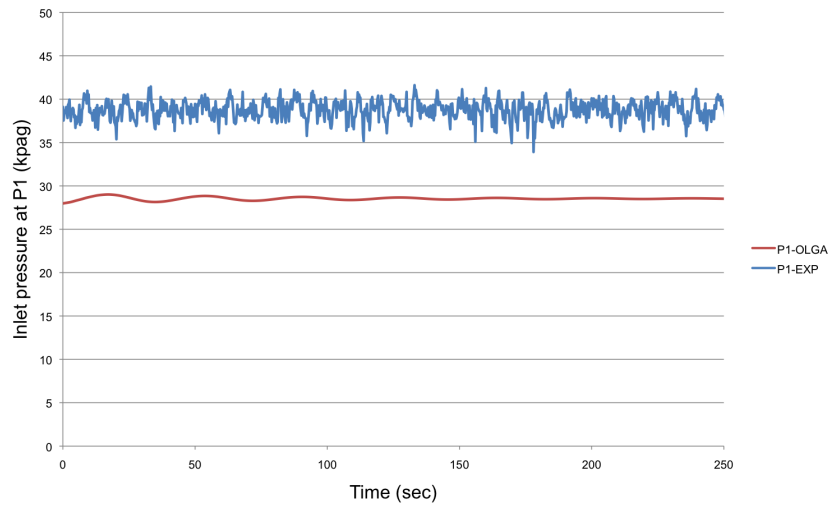


Figure 6.4: Comparison of simulation and experimental results of continuous flow. The liquid flow rate is 20 l/min and the gas flow rate 5 l/min.

The inlet pressure from the simulation started off oscillating, but settled down to a constant value after some time. In addition to the different pressure levels, the simulation results showed a much smoother plot than the experimental results. At inlet water flow rates above 10 l/min, the variance of the flow rate started to increase in the experiment, causing a disturbance in the inlet pressure measurements. In figure 6.4, the liquid flow rate was set to 20 l/min, but the difference in the maximum and minimum flow during this experiment was 8 l/min. This explains why the simulator showed values that were smoother: The inlet water flow rate in OLGA was a constant value.

In section 4.2.4, the pressure in the buffer tank was plotted for three different gas flow rates for varying the water flow rate. Figure 6.5 compares the pressure in the buffer tank from the experiment to the simulated results. Figure 4.10 is illustrated again to easier compare the results. The buffer tank pressures for three different gas flow rates from 3 l/min to 5 l/min are given in figures 6.5a and 6.5b.

The different gas velocities have separate markers; 3 l/min are marked by squares, 4 l/min as triangles and 5 l/min as stars. The maximum pressure has the color blue, the minimum pressure is marked in red and amplitude of the pressure in the buffer tank is marked in green.

Plot 6.5 can be used to find the point where the slugging flow moves from type I to type II.

In the type I region, the amplitude is large and the periods long, while in the slugging type II region, the amplitudes are smaller and periods shorter. As stated in section 4.2.4, the transition could be found at 0.26 m/s (or 5 l/min) for the miniloop experiment. Studying the results from the OLGA simulation, the transition does not occur before the liquid flow velocity has reached 0.64 m/s (or 12 l/min). This indicates that the severe slugging type I region in the flow regime map is larger for the OLGA simulations.

When studying the results from OLGA, it is easier to identify the behavior of the flow regimes at different liquid flow velocities. The six lowest points of liquid flow were in the severe slugging type I region. As mentioned earlier, the amplitude remained constant when the liquid flow rate remained constant and the gas flow rate varied. This corresponds with the simulation results in figure 6.5b. The flow regime started to change at 0.5 m/s. The minimum pressure remained equal for all the gas flow velocities, but the maximum pressure changed. The highest gas flow rate gave the higher maximum pressure in the buffer tank.

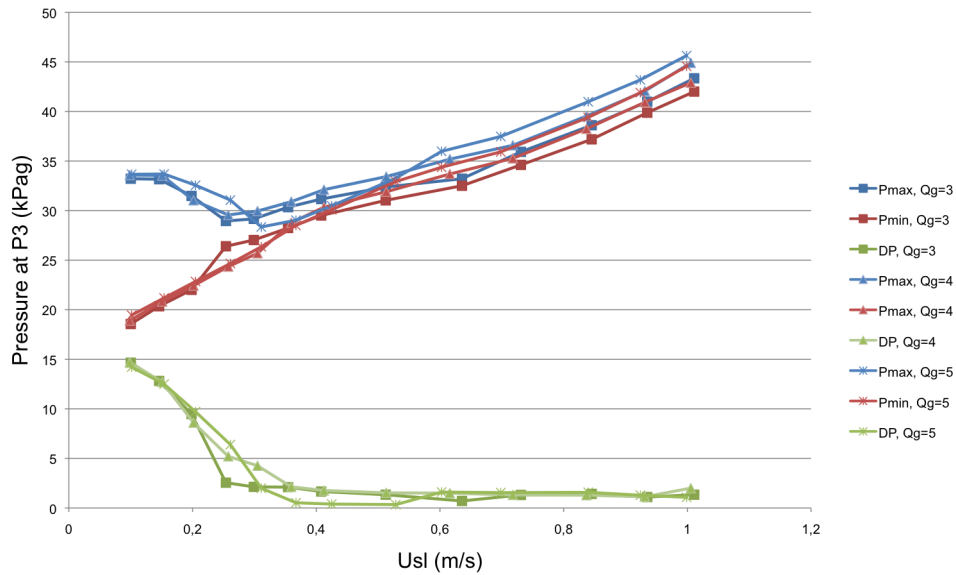
The amplitude decreased at a lower rate with increasing gas flow velocity. This was observed for both the experimental and simulated results in figure 6.5.

The conclusion of this comparison is that the severe slugging type I region is extended to higher liquid flow velocities in the simulator compared to the experimental setup. In figure 6.6 and 6.7, the liquid flow is held constant at 3 l/min. This plot is also illustrated in section 4.2.4 for the open-loop experimental data, here these values are compared to the simulation results from OLGA. Figure 6.6 is a plot of the maximum and minimum pressure at the inlet. The experimental data is marked by squares and the simulation results are marked with stars. The blue line represents the maximum pressure and the red line represents the minimum pressure.

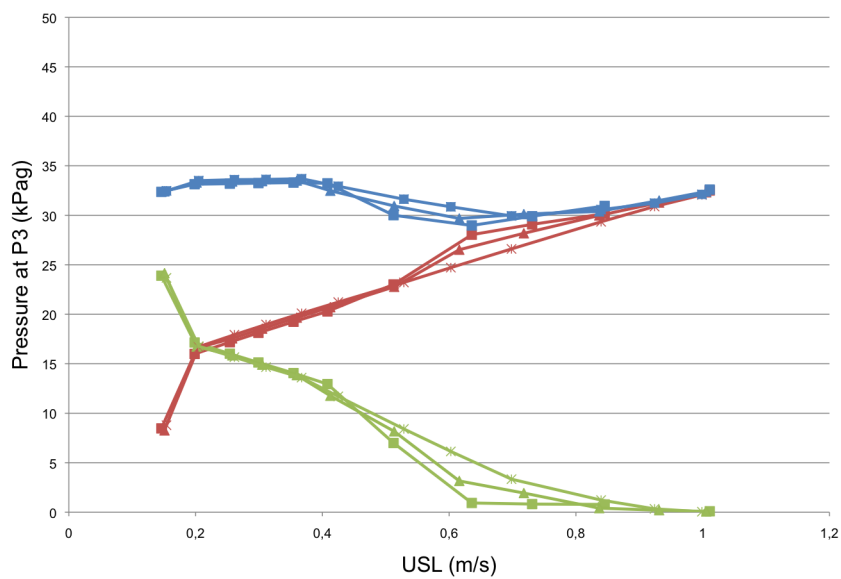
Both the experimental data and the OLGA simulations show that the amplitude remained constant in the severe slugging type I region when the liquid flow rate was not changed. However, the boundary of the severe slugging region was pushed to the right in the OLGA simulations. The boundary for severe slugging type I in figure 6.6 was at a gas flow velocity of 0.35 m/s in the experiment, and 0.5 m/s in the simulation for this specific water flow rate. When performing the simulations, it became apparent that the model did not show the hydrodynamic or transition flow regime. The flow regime from the simulations moved directly from severe slugging type I to continuous flow when increasing the gas flow rate. This can also be observed in the period plot in figure 6.7. The experimental results are marked by purple squares and the output from the simulation is marked by green stars. While the period between slugs in the experiment decreased steadily, the period from the simulation jumped from 55 seconds to zero at a gas flow velocity of 0.53 m/s.

It is hard to tell the difference between severe slugging and hydrodynamic slugging in the model. Hydrodynamic slugs are initiated in the horizontal section of the pipe. The base case this model was developed from is used for verification of severe slugging. A slug tracking model is required to see where the slugs are initiated in the model.

All the points simulated in OLGA are compared to the experimental data in appendix H. Comparisons were made on the slugging period, the buffer tank pressure amplitude and the flow regime.



(a) Results from miniloop experiment.



(b) Results from OLGA simulation

Figure 6.5: Comparison of the pressure in the buffer tank (P3) for different gas flow rates in experiment and in OLGA.

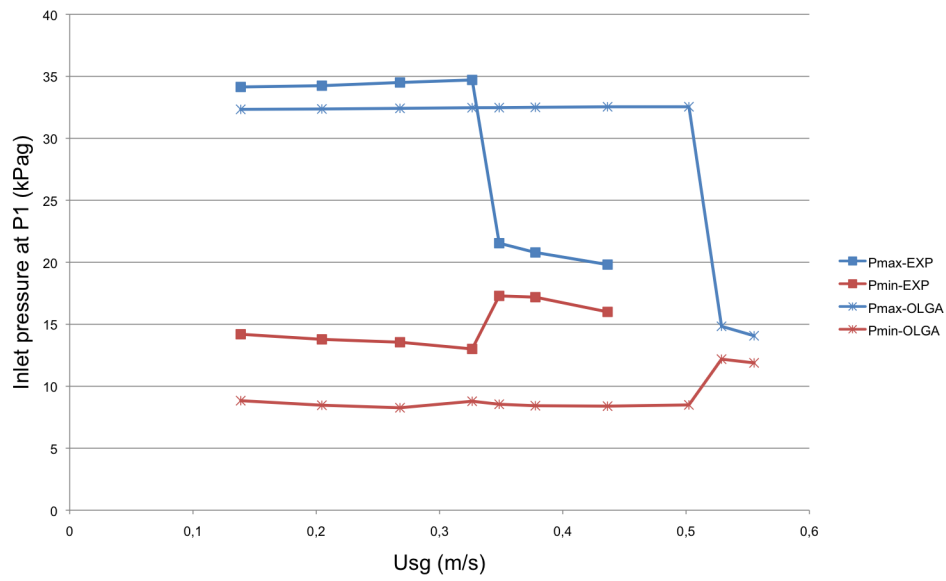


Figure 6.6: Comparison of simulation and experimental results of inlet pressure with constant liquid flow of 3 l/min.

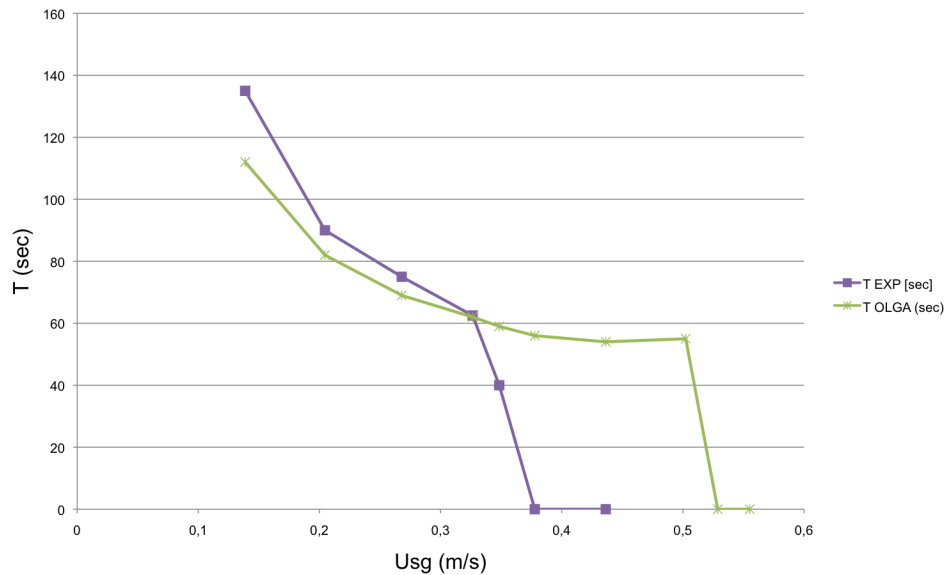


Figure 6.7: Comparison of simulation and experimental results of period between slugging with constant liquid flow of 3 l/min.



# Chapter 7

## Further work

The scope of this thesis was to document the complete flow regime map for the miniloop, and compare the open-loop and closed-loop results. Some ideas for further work on the miniloop are given below:

- Test different control structures for the points that were not stabilized in the closed-loop experiment:
  - Test different controlled variables, for example the pressure in the buffer tank, at the top of the riser or at the low point of the riser. In the last case, a pressure sensor must be added at the low point.
  - Test cascade control with differential pressure in the inner loop and the inlet pressure in the outer loop. In this case, a differential pressure sensor must be added to the experimental setup.
- Replace the pipe between the buffer tank and the inlet with a larger diameter pipe to decrease the pressure drop from buffer tank to inlet.
- Increase the height of the riser to study the dynamics of expansion driven instabilities in long risers.
- Improve the OLGA model to better fit the experimental data.
- Add a controller to the OLGA-model to compare the closed-loop experimental data with the model.
- Compare the experimental data enclosed in appendix A with other simplified models.



## Chapter 8

# Conclusion

The conclusion from studying the flow regime map is that riser slugging occurs with different flow patterns depending on the flow rate of the two phases. When both the liquid and gas flow rate was low, severe slugging type I occurred. This slugging was identified with long periods between the slugs and large pressure build up in the buffer tank before blowout. The whole riser was filled with liquid at each cycle.

When the liquid flow is increased, the period between each cycle decreased. The average pressure in the buffer tanks was higher, but the amplitude of the pressure variations were smaller. This was labeled severe slugging type II. Gas bubbles escaped through the blockage during liquid build up in the riser, breaking up the riser slugs and decreasing the period.

The feedback controller with the inlet pressure as the controlled variable proved to be effective in the severe slugging type I region. However, when the gas flow rate became too low, the controller was not able to stabilize the flow regime because the choke valve closed almost completely in order to increase the upstream pressure. In the severe slugging type II region, the frequency between each slug became too high and the controller had no stabilizing effect. Because the periods between the slugs were short and the pressure amplitude low, it is possible for a facility to be constructed to handle this flow regime type. The P-controller was superior to the PD-controller, both for severe slugging type I and type II.

The experiment of constructing a bifurcation map illustrated how the dynamic controller increases the production rate compared to manually choking the top side valve. The "stable" region existed at a valve opening of 10 % or less when manually choking the valve, while the dynamic controller stabilized the flow regime at an opening of 30 %. Increasing the valve opening, decreases the liquid holdup upstream the valve.

The OLGA model results were comparable to the experimental results, the flow pattern was most similar in the experimental severe slugging type I region. The inlet pressure was higher, the periods between slugging longer and the pressure amplitude smaller for the experimental results. The amplitude of the pressure oscillations remained constant when keeping the liquid flow rate constant and the pressure amplitude decreased when increasing liquid flow rate increased. This was true for both the experimental and simulated results. A slug-tracking model is required to differentiate between severe slugging and hydrodynamic slugging.



# Bibliography

- [1] Kjetil Havre, Karl Ole Stornes, and Henrik Stray. *Taming slug flow in pipelines*. ABB review 4, 2000.
- [2] Jalal Fahadi. *Anti-slug control, an experimental approach*. Project, Department of Chemical Engineering, NTNU, Trondheim, 2007.
- [3] Florent Di Melfio, Glenn-Ole Kaasa, and Nicolas Petit. *A first principle model for multiphase slugging flow in vertical risers*. Jont 48th IEEE Conference on Decision and Control and 28th Chinese Control Conference, 2009.
- [4] John-Morten Godhavn, Mehrdad P. Fard, and Per H. Fuchs. *New slug control strategies, tuning rules and experimental results*. Elsevier Ltd., 2004.
- [5] Heidi Sivertsen and Sigurd Skogestad. *Anti-slug control experiments on a small-scale two-phase loop*. Elsevier Science B.V., 2005.
- [6] Z. Schmidt, J.P. Brill, and H. D. Beggs. Choking can eliminate severe pipeline slugging. *Oil and Gas Journal*, pages 230–238, 1980.
- [7] John-Morten Godhavn, Stig Strand, and Gunleiv Skofteland. *Increased oil production by advanced control of receiving facilities*. Statoil R&D Process Control, Trondheim, for International Federation for Automatic Control, 2005.
- [8] Espen Storakaas. *Stabilizing control and controllability: Control solutions to avoid slug flow in pipeline-riser systems*. PhD thesis, Department of Chemical Engineering, NTNU, Trondheim, 2005.
- [9] Morten Søndrol. *Anti-slug regulering. Eksperimentell uttesting og verifikasjon*. Master thesis, Department of Chemical Engineering, NTNU, Trondheim, 2005.
- [10] Yong Bai and Qiang Bai. *Subsea pipelines and risers*. Elsevier Ltd., 2005.
- [11] Z. Schmidt, J.P. Brill, and H. D. Beggs. Experimental study of severe slugging in a two-phase-flow pipeline - riser pipe system. *SPE Journal*, 20(5):407–414, 1980.
- [12] Y. Taitel. Stability of severe slugging. *International Journal of Multiphase Flow*, 12(2):203–217, 1986.
- [13] F. E. Jansen, O. Shoham, and Y. Taitel. The elimination of severe slugging - experiments and modeling. *International Journal of Multiphase Flow*, 22(6):1055–1072, 1996.
- [14] Dale E. Seborg, Thomas F. Edgar, and Duncan A. Mellichamp. *Process Dynamics and Control*. John Wiley & Sons, Inc., second edition, 2004.

- [15] Christie J. Geankoplis. *Transport Processes and Unit Operations*. Allyn and Bacon, Inc., 1978.
- [16] SPE group by dynamic. Olga gui user manual, version 6.0. User manual from the OLGA-software.

# Appendix A

## Raw data and calculations

The raw data and processed data is enclosed to a separate disc attached to the thesis. The files are separated into three main folders:

- miniloop: contains all the logged data from the miniloop experiments, both the open-loop and the closed-loop data are enclosed in this folder. This folder is divided into "Original" and "Modified" depending the experimental setup.
- OLGA: contains all the raw data produced from OLGA and the comparisons to the experimental data.
- Calculation: contains the excel files used when producing the flow regime map and the bifurcation map, and the calibrations.



## Appendix B

# Calibration Results and Calculations

### B.1 Real liquid flow velocity

Table B.1 gives the values from the experiment. The amount of water in the bucket was measured in grams and the time in minutes. These values were used to find the volume flow rate in liters per minute for each run. The density of water was assumed to be  $1000 \text{ kg/m}^3$  (or  $1 \text{ kg/dm}^3$ ) and  $1 \text{ dm}^3 = 1 \text{ liter}$ . The formula for liquid flow rate is:

$$Q_L(l/min) = \frac{m(kg)}{\rho(kg/dm^3)} \cdot \frac{1(liter)}{1dm^3} \cdot \frac{1}{time(min)} \quad (B.1)$$

Table B.1: Values from liquid calibration experiment.

Run	Time	Water mass (kg)	Flow rate (l/min)
1	0.875	1.5219	1.7400
2	0.767	1.2072	1.5746
3	1.055	2.1082	1.9983
4	1.005	2.3876	2.3757
5	1.005	3.2193	3.2033
6	0.968	4.2198	4.3608
7	0.956	5.0627	5.2957
8	0.905	5.622	6.2122
9	0.804	5.8362	7.2590

### B.2 Calibration of liquid flow meter

The equation in LabVIEW was given on the form  $y = mx + b$ , where  $y$  was the measured value given in LabVIEW,  $x$  was the voltage from the measurement devices and  $m$  and  $b$  were constants. To compare the real measurements to the results given in LabVIEW, the voltage at each step was calculated by rearranging equation for measured value:

$$x = \frac{y - b}{m} \quad (\text{B.2})$$

The original values for  $m$  and  $b$  were 3738.9 and -14.955. By using the measured values in LabView ( $y$ ), the voltage for each run could be found. These values are given in table B.2

Table B.2: Voltage for each run in liquid flow meter calibration.

Run	Measured $Q_L$ in LabView (l/min)	Voltage
1	0	0.00400
2	0	0.00400
3	1.6194	0.00443
4	2.1300	0.00457
5	2.9752	0.00480
6	4.3140	0.00515
7	5.2308	0.00540
8	6.2809	0.00568
9	7.3191	0.00596

These voltage values were used as  $x$ -values to plot the real liquid flow velocity against the LabVIEW values. By using the linear regression in excel for the real water velocities, the parameters  $m$  and  $b$  was found. The new values did not differ much from the original values, and they remained unchanged.

### B.3 Pressure calibration

The procedure to calibrate the pressure is described in section 3.3 in the report, and the voltage for each run was calculated with the same procedure as for the liquid flow meter calibration. Table B.3, B.4 and B.5 gives the pressure from the calibration instrument, the pressure measured in LabVIEW and the voltage for each run.

Table B.3: Real pressure, pressure from LabVIEW and voltage signal from P1 calibration.

Real pressure (kPag)	Pressure P1 from LabView (kPag)	Voltage from P1 signal
5	6.4833	0.4788
8	10.4243	0.6482
10	12.7524	0.7484
12	15.7034	0.8752
15	19.5962	1.0426
18	23.5650	1.2133
20	26.1680	1.3252
23	30.1674	1.4972
25	32.7102	1.6065
30	39.4188	1.8950
35	46.0439	2.1799
40	52.6918	2.4657
45	59.3305	2.7512
50	65.9726	3.0368

Table B.4: Real pressure, pressure from LabVIEW and voltage signal from P2 calibration.

Real pressure (kPag)	Pressure P2 from LabView (kPag)	Voltage from P1 signal
5	6.2223	0.4676
8	10.1667	0.6372
10	12.4492	0.7353
12	15.3412	0.8597
15	19.2160	1.0263
18	23.1107	1.1938
20	25.7084	1.3055
23	29.6695	1.4758
25	32.1935	1.5843
30	38.8828	1.8720
35	45.4932	2.1562
40	52.1464	2.4423
45	58.8086	2.7288
50	65.4867	3.0159

Table B.5: Real pressure, pressure from LabVIEW and voltage signal from P3 calibration.

Real pressure (kPag)	Pressure P3 from LabView (kPag)	Voltage from P3 signal
5	6.2055	0.4668
8	9.9160	0.6264
10	11.9605	0.7143
12	14.5251	0.8246
15	18.1891	0.9821
18	21.9988	1.1459
20	24.5785	1.2569
23	28.5149	1.4261
25	31.0211	1.5339
30	37.6713	1.8199
35	44.2669	2.1035
40	50.9105	2.3892
45	57.5689	2.6755
50	64.2520	2.9628

## Appendix C

# Calculation of frictional pressure drop in pipe between buffer tank and mixing point

The equation for pressure drop caused by friction in the pipes is derived from the Fanning friction factor,  $f$ . This factor is defined as the drag force per wetted surface area over the product density times velocity head. The equation for the friction factor is given by: [15]

$$f = \left( \frac{\Delta p_f \pi R^2}{2\pi RL} \right) / \left( \frac{\rho v^2}{2} \right) \quad (\text{C.1})$$

Reforming equation C.1 to find the pressure drop gives:

$$\Delta p = 4 \cdot f \cdot \rho \cdot \frac{v^2}{2} \cdot \frac{L}{D} \quad (\text{C.2})$$

By using the correlation  $4f \approx \lambda$  for turbulent flow, the equation can be written as following:

$$\Delta p = \lambda \cdot \rho \cdot \frac{v^2}{2} \cdot \frac{L}{D} \quad (\text{C.3})$$

where the parameters and values for this calculation are:

- $\Delta p$  is the frictional pressure loss (Pa)
- $\lambda = 0.3 N_{Re}^{-0.25}$
- $N_{Re} = \frac{\rho v L}{\mu}$
- $\rho$  is the density ( $\text{kg/m}^3$ ) = 1.204 ( $\text{kg/m}^3$ )
- $v$  is the velocity of the flow (m/s) = 6.67 (m/s)

- L is the length of the pipe (m) = 6.4 (m)
- $\mu$  is the dynamic viscosity (kg/m s) =  $1.78 \cdot 10^{-5}$  (kg / (m s))
- D the diameter of the pipe (m) = 0.004 (m)

The Reynold's number:

$$N_{Re} = \frac{1.204(\text{kg}/\text{m}^3) \cdot 6.67(\text{m}/\text{s}) \cdot 6.4(\text{m})}{1.78 \cdot 10^{-5}(\text{kg}/(\text{m}\cdot\text{s}))} = 2887436 \quad (\text{C.4})$$

Which gives:

$$\lambda = 0.3 \cdot 2887436^{-0.25} = 0.0073 \quad (\text{C.5})$$

The pressure drop due to friction is calculated to be:

$$\Delta p = 0.0073 \cdot 1.204(\text{kg}/\text{m}^3) \cdot \frac{6.67^2(\text{m}/\text{s})^2}{2} \cdot \frac{6.4(\text{m})}{0.004(\text{m})} = 312(\text{Pa}) \quad (\text{C.6})$$

## Appendix D

# Results and Calculation of the Flow Map

### D.1 Conversion to standard conditions

An example of converting water and gas flow rate from liters per minute to meters per section is given in this appendix. The values are taken from the experiment with the modified setup. In this example the water flow rate of 10 l/min and a gas flow rate from 1-7 l/min will be converted.

The conversion of water was straight forward because it was assumed that water is an incompressible fluid, meaning that the pressure does not effect the volume flow of water. However, when converting the flow rate of air, the value must first be converted to standard conditions. The parameters used in this conversion are:

Table D.1: Parameters used for conversion of liquid flow

Parameter	value
Standard pressure (atm)	1
Standard temperature (K)	293
Ambient temperature during experiment (K)	295
Diameter pipe (m)	0.02
Cross section area of pipe (m <sup>2</sup> )	0.00031416
10 <sup>5</sup> pascal in atmosphere (atm)	0.986923169

The formula for converting the flow rate of liquid to m/s is given by:

$$Usl(m/s) = Q_L(l/min) \cdot \frac{1(min)}{60(sec)} \cdot \frac{1(dm^3)}{1(l)} \cdot \frac{1(m^3)}{1000(dm^3)} \cdot \frac{1}{A(m^2)} \quad (D.1)$$

When constructing the flow regime map, the average water flow rate was used. Table D.2 gives the seven average values at 10 l/min that was used at the different gas flow rates. The values in

the table are given in l/min and in m/s.

Table D.2: Conversion of liquid volume flow to the liquid flow velocity

$Q_G$ (l/min)	Average $Q_L$ (l/min)	Usl (m/s)
1	10.0294	0.5321
2	9.9791	0.5294
3	9.9628	0.5285
4	9.6741	0.5132
5	9.6562	0.5122
6	9.7000	0.5146
7	9.8206	0.5210

As described in section 4.2.3 in the report, the ideal gas law was used to convert the gas flow rate into standard conditions. The volume flow rate of air depended on the pressure at the inlet. First the pressure was converted from kPag to atmospheric pressure. The next step was to convert the gas flow rate into standard conditions using equation 4.4, and finally converting the flow rate into meters per second by the same equation at for the liquid flow rate:

$$U_{sg}(m/s) = Q_{G,STD}(l/min) \cdot \frac{1(min)}{60(sec)} \cdot \frac{1(dm^3)}{1(l)} \cdot \frac{1(m^3)}{1000(dm^3)} \cdot \frac{1}{A(m^2)} \quad (D.2)$$

Table D.3 gives the gas flow rates from 1-7 l/min at the liquid flow rate of 10 l/min.

Table D.3: Conversion of gas volume flow to the gas flow velocity

$Q_G$ (l/min)	P1 (kPag)	P1 (atm)	$Q_{G,STD}$ (l/min)	Usg (m/s)
7	28.2546	1.2658	0.00014918	0,474840244
6	28.8600	1.2717	0.00012847	0,408927103
5	29.5435	1.2785	0.00010763	0,342580027
4	29.7382	1.2804	8.6229E-05	0,274476043
3	29.8639	1.2817	6.4735E-05	0,206056348
2	29.6378	1.2794	4.3081E-05	0,137131787
1	30.0595	1.2836	2.1611E-05	0,068788932

## Appendix E

# Deviation errors in the liquid flow velocities

### E.1 Deviation errors during liquid flow calibration

If the accuracy of the time taking during the liquid calibration is assumed to be 1 second. Table E.1 gives the error for each run in during the calibration. The errors are given in (l/min), the error normalized for 1 l/min and the error in (m/s).

Table E.1: The deviation errors during liquid calibration

Measured velocity (l/min)	Error (l/min)	Error per liter (l/min)	Error (m/s)
1.9983	$\pm 0.0311$	$\pm 0.0156$	$\pm 0.00165$
2.3757	$\pm 0.0388$	$\pm 0.0163$	$\pm 0.00206$
3.2033	$\pm 0.0523$	$\pm 0.0163$	$\pm 0.00277$
4.3608	$\pm 0.0738$	$\pm 0.0169$	$\pm 0.00392$
5.2957	$\pm 0.0907$	$\pm 0.0171$	$\pm 0.00481$
6.2122	$\pm 0.1123$	$\pm 0.0180$	$\pm 0.00596$
7.2590	$\pm 0.1474$	$\pm 0.0203$	$\pm 0.00782$
1.7400	$\pm 0.0325$	$\pm 0.0187$	$\pm 0.00173$
1.5746	$\pm 0.0335$	$\pm 0.0213$	$\pm 0.00178$

The maximum change in the LabVIEW equation would be  $y = 3314,7x + 12,727$  compared to  $3456,3x - 13.383$ , which would not have a large effect on the liquid flow velocities logged in LabView.

### E.2 Deviation errors of experimental results

When the liquid flow rate increased, the variations also increased. Table E.2 gives the liquid flow rates and deviations at a gas flow rate of 7 l/min. At this gas flow rate the flow regime was

constant for all liquid flow rates. The intended values, the average values from LabVIEW and the deviations in liters per minute and in percentages of average liquid flow rates are given in the following table.

Table E.2: The deviation in liquid flow rate at different values

Intended $Q_L$ (l/min)	Average $Q_L$ (l/min)	Deviation of $Q_L$ (l/min)	Deviation of $Q_L$ (%)
2	2.062	$\pm 0.120$	$\pm 5.84$
4	3.976	$\pm 0.153$	$\pm 3.9$
6	5.998	$\pm 0.153$	$\pm 2.6$
8	8.101	$\pm 0.230$	$\pm 2.8$
10	10.029	$\pm 0.186$	$\pm 1.9$
12	12.055	$\pm 0.690$	$\pm 5.7$
14	13.661	$\pm 1.151$	$\pm 8.4$
16	15.798	$\pm 2.400$	$\pm 15.2$
18	17.399	$\pm 2.684$	$\pm 15.4$
20	18.759	$\pm 3.714$	$\pm 19.79$

# Appendix F

## Block Diagram in LabVIEW

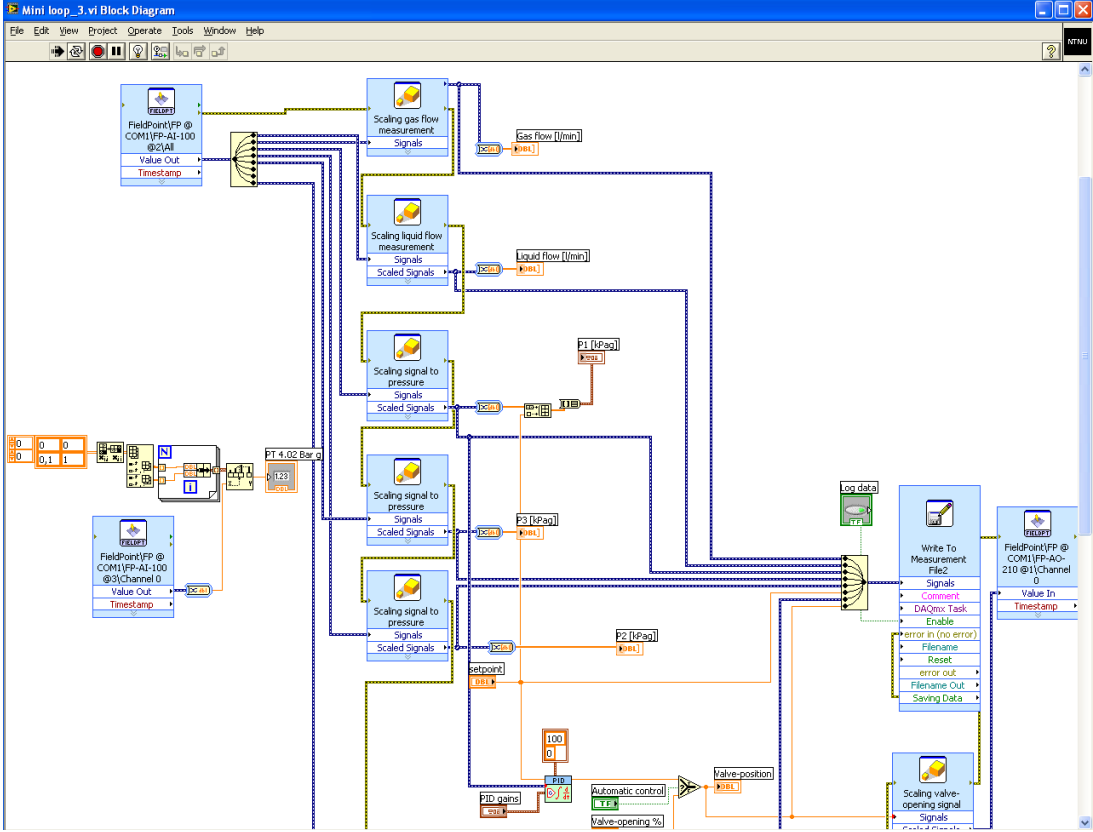


Figure F.1: Blockdiagram in LabVIEW



## Appendix G

# A description of the OLGA base case for severe slugging.

The base case model in OLGA for severe slugging was a two-phase model consisting of oil and gas. The geometry of the riser system is given in table G.1. The minimum and maximum section length was set to 100 m and 200 m in the base case model.

Table G.1: Geometry of severe slugging base case model in OLGA.

Pipe no.	Diameter (m)	Length (m)	Elevation (m)
1	0.12	2000	0
2	0.12	2000	-34.9
3	0.12	300	-5.24
4	0.1	300	300
5	0.1	100	0

This riser system was a much larger system than the miniloop riser. The geometry was changed to the setup illustrated in section 3.

In the base case the inlet consisted of one source with an oil and gas mixture. The input values in the base case are given in table G.2.

Table G.2: Inputs to the severe slugging base case model in OLGA.

Input	Value
Outlet pressure	50.1bar
Ambient temperature	6°C
Inlet gas flow rate	4kg/s
Inlet oil flow rate	15 kg/s
Inlet temperature	62°C
Valve opening	100%

The valve was positioned at the horizontal section at the top of the riser (pipe 5).



## Appendix H

# Comparison of experimental and modeling results.

In figures H.1 and H.2 the results from the experiment are compared with the values from the simulation. The parameters in these tables are:

- $Q_L$  and  $Q_G$  are the volumetric inlet flow rate of liquid and gas (l/min)
- $U_{SG}$  and  $U_{SL}$  are the inlet velocity of liquid and gas (m/s)
- $T$  is the period between the slugs (sec)
- $P3$  Amp is the pressure amplitude in the buffer tank (kPag)
- **Regime** is what flow regime exists at the certain conditions

Experimental results										OLGA-Model		
$Q_L$ (l/min)	$Q_G$ (l/min)	$U_{SL}$ (m/s)	$U_{SG}$ (m/s)	T (sec)	P3 Amp (kPag)	Regime	T (sec)	P3 Amp (kPag)	Regime			
4	2	0.20	0.14	114	10.82	SS I	106	17.25	SS I			
4	3	0.20	0.20	66	9.47	SS I	78	17.15	SS I			
4	4	0.20	0.26	56	8.61	SS I	64	16.73	SS I			
4	5	0.20	0.32	59	9.71	Transition	57	16.78	SS I			
5	2	0.25	0.14	22	7.76	SS II	98	16.14	SS I			
5	3	0.25	0.20	16	2.55	SS II	73	16.02	SS I			
5	4	0.26	0.27	53	5.21	SS II	60	15.85	SS I			
5	5	0.26	0.33	51	6.39	Hydrodynamic	54	15.67	SS I			
6	2	0.30	0.14	17	2.03	SS II	94	15.26	SS I			
6	3	0.30	0.20	13	2.13	SS II	69	15.13	SS I			
6	4	0.31	0.27	80	4.26	Transition	58	14.91	SS I			
6	5	0.31	0.33	39	6.39	Hydrodynamic	51	14.66	SS I			
7	2	0.35	0.14	17	1.68	SS II	87	14.14	SS I			
7	3	0.35	0.21	12	2.10	SS II	64	14.06	SS I			
7	4	0.36	0.27	10	2.13	SS II	53	13.85	SS I			
7	5	0.37	0.33	-	0.53	Continuous	47	13.60	SS I			
8	2	0.41	0.14	12	1.34	SS II	79	13.06	SS I			
8	3	0.41	0.21	9.5	1.66	SS II	55	12.95	SS I			
8	4	0.41	0.27	9	1.76	SS II	46	11.76	SS I			
8	5	0.42	0.34	-	0.39	Continuous	42	11.70	SS I			
10	2	0.51	0.14	9.5	1.00	SS II	9	1.55	SS II			
10	3	0.51	0.21	8.5	1.26	SS II	43	6.99	SS I			
10	4	0.51	0.27	8	1.53	SS II	38	8.17	SS I			
10	5	0.53	0.34	-	0.34	Continuous	35	8.41	SS I			
12	2	0.63	0.14	-	0.71	Bubble	7	0.90	SS II			
12	3	0.64	0.21	-	0.71	Bubble	6	0.93	SS II			
12	4	0.62	0.28	7	1.50	SS II	7	3.15	SS II			
12	5	0.60	0.35	7	1.66	SS II	33	6.14	SS I			

Figure H.1: Table of OLGA and experimental comparisons.

Experimental results										OLGA-Model		
Q <sub>L</sub> (l/min)	Q <sub>G</sub> (l/min)	U <sub>SL</sub> (m/s)	U <sub>SG</sub> (m/s)	T (sec)	P3 Amp (kPag)	Regime	T (sec)	P3 Amp (kPag)	Regime			
14	2	0.7	0.14	-	0.87	Bubble	7	0.88	SS II			
14	3	0.73	0.21	-	1.32	Bubble	6	0.82	SS II			
14	4	0.72	0.28	8	1.32	Transition	6	1.94	SS II			
14	5	0.70	0.35	6	1.55	SS II	40	3.34	SS I			
16	2	0.85	0.14	-	-	Bubble	-	-	-			
16	3	0.85	0.22	-	1.42	Bubble	5	0.79	SS I			
16	4	0.84	0.29	4	1.30	Transition	4	0.41	SS I			
16	5	0.84	0.36	4	1.58	SS II	39	1.23	SS II			
18	2	0.94	0.15	-	1.03	Bubble	-	0.26	Stable			
18	3	0.94	0.22	-	-	Bubble	-	-	-			
18	4	0.93	0.29	-	1.05	Transition	-	0.21	Stable			
18	5	0.92	0.37	-	1.29	Transition	-	0.34	Stable			
20	2	1.01	0.15	-	1.45	Bubble	-	0.16	Stable			
20	3	1.01	0.22	-	1.21	Bubble	-	0.10	Stable			
20	4	1.01	0.29	-	1.81	Transition	-	0.08	Stable			
20	5	1.00	0.37	-	1.08	Transition	-	0.05	Stable			

Figure H.2: Continued table of OLGA and experimental comparisons.